Bachelor Thesis

Bi-Static Sense and Avoid System for Drones (BiSAD)–Signal Design

Group H

TU Delft

Bachelor Thesis

Bi-Static Sense and Avoid System for Drones (BiSAD)–Signal Design

by

Mohammed Abo Alainein,
Ossama El Boustani

in partial fulfilment of the requirements for the degree of

Bachelor of Science

in Electrical Engineering

at the Delft University of Technology,
to be defended publicly on Monday June 29, 2020 at 12:30 PM.

Student:	Mohammed Abo Alainein (4570081),
Student:	Ossama El Boustani (4542274)
Project supervisor:	Dr. F. Uysal, TU Delft
Thesis committee:	Prof. dr. ir. G.J.T. Leus, TU Delft
	Dr. F. Uysal, TU Delft
	Dr. D. Cavallo, TU Delft
	Dr. O. Dogan, TU Delft

TU Delft

Abstract

This thesis describes the waveform design of a bi-static radar system and its implementation with Software Design Radio, SDR for short. The system is designed for Selfly ED&A and is intended to be used by Wings for Aid. Wings for Aid develops an airborne aid-delivery system to be used in disaster areas. The radar system can be mounted on the delivery drones and used to detect other drones and obstacles to avoid collisions.
The thesis focuses mainly on the radar waveform design. In addition, the thesis provides analysis of the radar system performance and system implementation with commercial off the shelf SDR. A proof of concept has been realised by means of simulations using the open source software GNU Radio Companion.

Preface

In the context of the Bachelor Graduation Project at the Delft University of Technology Department of Electrical Engineering, Mathematics and Computer Science, we have been tasked with a project to design prototype of a bi-static radar for the company Selfly ED&A (based in Noordwijk, the Netherlands). We have been working on the project in a team of six students from April 20, 2020 to June 25, 2020. This is thesis is written to fulfil the requirements of the Bachelor Graduation Project. Our contribution to the project was to propose an optimal radar waveform, recommend a Software Defined Radio device for the implementation of the prototype, and simulate the design using open source software. The project was proposed by Ronald van Gent (Selfly ED&A) and supervised by Dr. Faruk Uysal (Delft University of Technology).

Working on a project remotely in the midst of the Covid-19 pandemic while in lockdown was not easy. System engineering and coordination with a group of students was therefore even more complicated. Nonetheless, motivation and team spirit was absolutely present during the project. We would like to thank Ronald van Gent for proposing the project and Dr. Faruk Uysal for his supervision and guidance. We also would like to thank Dr. Ozan Dogan (Delft University of Technology) and Ir. Jerom Maas (Delft University of Technology) for their assistance. Finally, we would like to thank our teammates: Jeroen Blok, Job van der Kleij, Sander Renger and Marien Verseput for their contribution and jovial collaboration.

Mohammed Abo Alainein and Ossama El Boustani
Delft, June 2020

Contents

1 Introduction

Selfly ED&A aims to provide small aircraft with *electronic eyes*. So far, Selfly has developed equipment with easily available hardware and makes use of the presence of Terminal Approach Radars (TAR) that already exist on the ground. All this hardware, including the broadcast signal, is neither designed nor optimised for this application. For the Bachelor Graduation Project at the Department of Electrical Engineering (EE3L11 BAP 2019/2020), we propose a design of the transmitter, receiver and waveform for a bi-static radar that Selfly can use for automated delivery drone of its customer Wings for Aid that facilitate airborne delivery service to emergency-struck areas.
The system is called Bi-Static Sense and Avoid System for Drones, abbreviated as BiSAD, and is based on the concept of having one "mother-ship" that transmits radar pulses around multiple smaller drones equipped with receiver antennas. These pulses are intercepted by the smaller drones causing echoes. Based on the transmitted pulses and echos, the drones location can be estimated. The radar system is implemented using Software Defined Radio (SDR).
This chapter provides a short state of the art analysis, the problem definition, the system overview and the layout of the thesis.

1.1. State of the Art Analysis

Bi-static radars unlike conventional—or rather monostatic—radars have transmitter and receiver antennas physically separated by a substantial distance. Research on and development of bi-static radars dates back to World War 2 (WW2). The Germans had a Passive Bi-staic Radar (PBR) called Klein Heidelberg for air defence exploiting transmissions from the British Chain Home (CH) radar transmitter [6]. Due to the fact that Klein Heidelberg had no transmitting antennas, it was completely hidden and the Allies did not discover its existence until after the D-Day landings.

SDRs come in different shapes and sizes, making it easier to produce fast prototypes of or even complete systems. As more drones hit to the sky, new technology is needed to maintain air safety or preform security or surveillance tasks [10]. Kwag et al. have proposed a small scale ground based monostatic radar solution that can be used for done detection in [9, 10]. This monostatic radar exploits FMCW waveforms and is multi-band (S-, X- and K-band). Another example of the application of SDR based radar for detection of air-vehicles is presented by Moore in [13]. The work presents a prototype of radar to detects (in S-band) unmanned air-vehicle and track them (in X-band). The prototype is produced with commercially available hardware components. The total cost of the prototype is $5,000.

1.2. Problem Definition

As the idea of delivery drones is continuously gaining popularity, there is also a need for automation. The project owner Selfly ED&A aims develop an on board Bi-static Sense and Avoid for Drones (BiSAD). This obstacle detection system uses radar to scan the environment during flight. BiSAD exploits bi-static radar mainly because the system should be dynamic an reliable even after natural disaster scenario where an area is completely devastated such that even air-traffic control is no longer available. Since BiSAD intended for delivery drones, using a bi-static radar with a powerful airborne illuminator reduces the weight of the Sense and

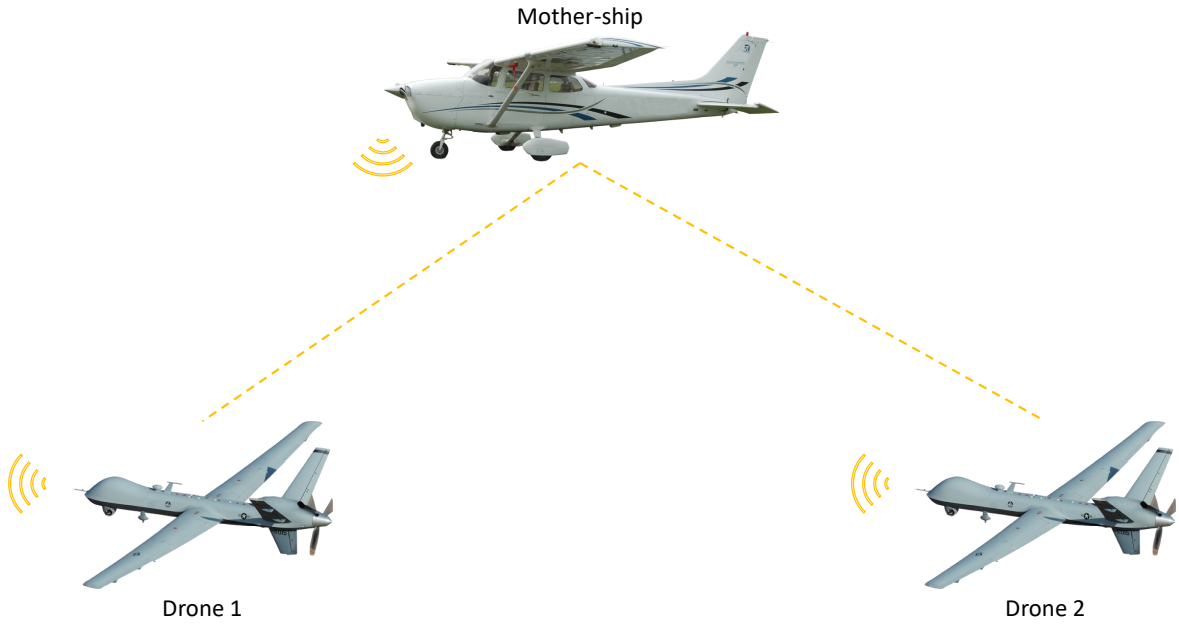

Figure 1.1: A visualisation of the concept of Bi-static Sense and Avoid for Drones (BiSAD).

Avoid System and allows the drones to carry more payload. BiSAD consists of a radar transmitter and multiple receivers, depending on the number of drones (see Figure 1.1). The mother-ship would fly and transmit radar waves and the drones would intercept these wave as they get reflected off buildings and airborne obstacles.

Existing drone delivery services, e.g. the California based Zipline [1], rely on GPS navigation and air traffic control. Even though Zipline drones fly autonomously, they still rely on air traffic control. Providing autonomously flown drones with a sense and avoid system adds another level of autonomy. Currently, Selfly ED&A makes use of the presence of Terminal Approach Radars (TAR) that already exist on the ground as transmitters and the drones are equipped with receivers. The goal is to design a complete airborne bi-static radar system. To achieve this goal, the design of a transmitter chain, receiver chain and a radar waveform is outsourced as a Bachelor Graduation Project ("BAP"). The BAP is subdivided into three separate assignments:

1. Design of a transmitter antenna system using off the shelf software defined radio equipment.
2. Design of an optimal signal to use for the application implementing within the software defined radio.
3. Design of a twin-receiver antenna, using off the shelf equipment, to determine vertical direction of arrival (DoA).

The three assignments are assigned to three different groups, each consisting of two students. The project is planned to be completed during the 4^{th} academic quarter (Q4) of the academic year 2019/2020. The budget for system should be kept below €52,000, i.e. the transmitter chain total price of components is limited at €50,000, and the receiver chain total price of components is limited at €2,000. However, this project aims to provide a proof of concept. The budget is therefore limited to €2,000 for both the transmitter and receiver chain.

1.3. System overview

Figures 1.2 and 1.3 show a high level block diagram of the transmitter and receiver systems. The frequency band in which the radar system will transmit and receive is the X-band. The host-PC in the transmitter system generates the radar waveform and programs the SDR using GNU radio companion software. The generated radar waveform lies in the S-band and is relayed to the transmitter chain. The chain is responsible to upconvert the signal to the X-band. The second output of the SDR provides the local oscillator needed for up-conversion. Furthermore, the signal is filtered and amplified before transmission.

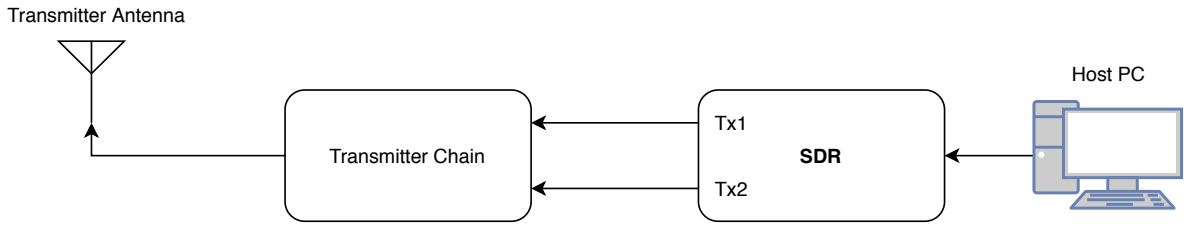

Figure 1.2: High-level block diagram of the transmitter system.

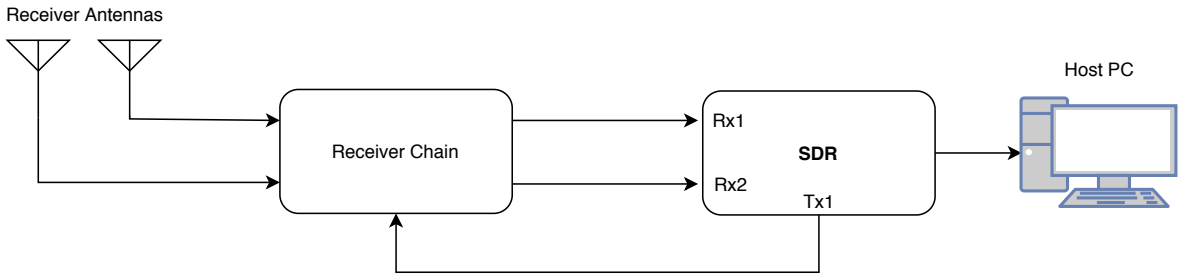

Figure 1.3: High-level block diagram of the receiver system.

At the receiver side, the radar waveform is down-converted to the S-band. Similarly, the SDR provides the needed local oscillator. Furthermore, the receiver chain provides filtering and amplification to the signal. The signal is then relayed to the SDR and a host-PC. The host-PC implements the needed signal processing for range and AOA detection algorithms using GNU radio software.

1.4. Thesis Layout

This thesis is essentially structured such as related theory is discussed, the design is elaborated, and finally a conclusion to conclude the thesis. Nonetheless, after this chapter, first a Program of Requirements is provided in Chapter 2. The Program of Requirements include system requirements and requirements related to radar signal design. Chapter 3 presents the related theory. Chapter 3 discusses the geometry of the bi-static radar in Section 3.1 and the range resolution for bi-static radar in Section 3.2. Moreover, the Doppler effect in radar measurements is discussed in Section 3.3. In addition, Chapter 3 discusses the radar equation in Section 3.4 and introduces the concept of Cassini ovals in Section 3.5. Thereafter, Chapter 4 provides an introduction to radar waveforms in Section 4.1. Section 4.2 discuss the mathematical representation of the radar waveform proposed in this thesis. Section 4.3 discusses the concept of matched filtering and Section 4.4 introduces pulse compression and presents some examples of pulse compression techniques. Chapter 5 provides an overview of the systems and discuss Software Defined Radio. Chapter 6 provides a system evaluation based on simulation results. First, Section 6.1 discusses the range resolution. Second, Section 6.2 discusses the blind range inherent to bi-static radar. Furthermore, Section 6.3 provides an analysis of range accuracy, and Section 6.4 evaluates the SNR using ovals of Cassini. Finally, Chapter 7, discusses the simulation of the radar system implemented in GNU Radio.

2

Program of Requirements

General Requirements

The Bi-Static Sense and Avoid System for Drones (BiSAD) includes a transmitter and receiver chain, and of course radar waveform or signal design. BiSAD is not merely composed of the three mentioned parts, the entire system includes a compunction link between drones and the mother-ship and software that implements localisation of the drones and the targets detected by the bi-static radar. The scope of the project is limited to the design of the transmitter and receiver chain and the radar waveform. The general requirements address these three parts of the Bi-Static Sense and Avoid System for Drones.

Assumptions

The scope of the project is limited to the design of the transmitter and receiver chain and the radar waveform. To simplify the project and ensure feasibility, especially during the COVID-19 pandemic, it is assumed that the project owner Selfly ED&A already has the software packages necessary to implement positioning of the mother-ship and drones using GPS and localising the targets on a Plan position Indicator (PPI) and visualising the targets on a map.

Mandatory Requirements

The mandatory requirements specify the requirements that ought to be complied with at all times. These are subdivided into two categories, functional requirements and non-functional requirements. The functional requirements describe what system/product does, and non-functional requirements describe attributes the system/product has got to have.

1. Non-functional Requirements

(a) The receiver must have reception of the direct-path from the transmitter up to 50 km.

(b) The receiver must have reception of echoes reflected from target within a radius of up to 5 km.

(c) The position of the reflection must be determined within 300 m accuracy.

(d) The system should be compatible with the requirements of Agentschap Telecom.

(e) The transmitter and receiver should be built with commercial of the shelf (COTS) equipment.

(f) The transmitter should use at most 3 kW of power.

(g) The transmitter should weigh at most 10 kg.

(h) The receiver is based on current Software Defined Radio capability.

This project aim to provide a proof of concept for the actual system. This means that all of the aforementioned requirements are the requirements apply to the desired system. For now, all the requirements, except for the first two, will be met and verified through simulations.

2. Functional Requirements

(a) The system should detect objects with the size of a C-172 aircraft and bigger within the range ($\sigma \geq 1\,\mathrm{m}^2$)

(b) The system should determine the Direction of Arrival (DoA).

(c) The system should determine the distance between receiver and targets.

Trade-off Requirements

(a) RF in X-band.

(b) IF in range supported by the selected SDR.

Signal Design Requirements

The signal design requirements address the desires and constraints with regard to the design of the radar waveform. The signal design requirements are subdivided into two categories too, non-functional and functional.

1. Non-functional Requirements

(a) The carrier frequency of the waveform should be 3.875 GHz.

(b) The bandwidth of the waveform should be feasible with commercial off the shelf components (SDR, antennas, filters and amplifiers).

(c) The waveform should yield a worst-case scenario range resolution no larger than 300 m.

(d) The waveform should be Doppler tolerant.

3

Bi-Static Radar Geometry and Equations

3.1. System Geometry and Isorange Contours

The bi-static radar is a system where the transmitter and receiver are separated by a distance comparable to the target distance. Figure 3.1 shows a two-dimensional system in the bi-static plane. The mother-ship is the drone where transmitter equipped with a rotating antenna is located and separated by a distance L from the receiver drone. The distance L is called the baseline. The target drone is separated by a distance R_t from the transmitter and distance R_r from the receiver. The angels θ_r and θ_t are the look angles of transmitter and receiver respectively, measured clockwise from North. The angle β is called the bi-static angle and from the geometry we have $\beta = \theta_t - \theta_r$.

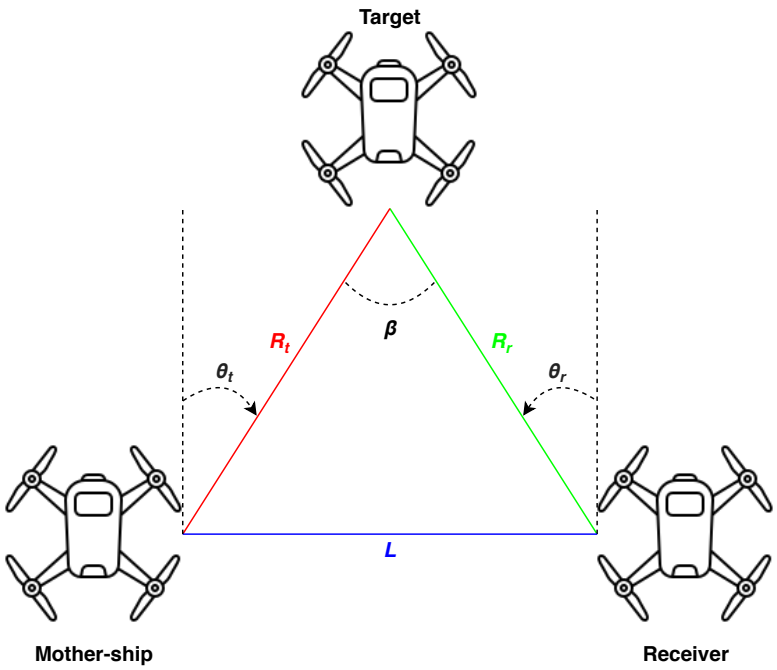

Figure 3.1: Bi-static Radar geometry.

The distance R_r is required for target detection. The mother-ship transmits RF pulses and the receiver drone will receive the direct path signal and the reflections from the target drone. The time difference ΔT between the direct path and the echo is related to the distances:

$$R_t + R_r = c\Delta T + L \tag{3.1}$$

Where c is the speed of light. Equation (3.1) results in a family of solutions for the range sum $(R_t + R_r)$ which traces out an ellipse. The focal points of the ellipse are the transmitter Tx and the receiver Rx sites. This

family of solution is called an isorange. For a fixed ΔT and L we have an isorange curve where at any point of the curve the range sum $(R_t + R_r)$ is constant. For a different ΔT or L we have different isorange curve. The equation for an ellipse with the origin located at the midpoint of the baseline is given by:

$$\frac{x}{a^2} + \frac{y^2}{b^2} = 1 \tag{3.2}$$

Where a is the semi-major axis of the ellipse and is:

$$a = \frac{R_t + R_r}{2} \tag{3.3}$$

And b is the semi-minor axis of the ellipse:

$$b = \sqrt{a^2 - \frac{L^2}{4}} \tag{3.4}$$

Figure 3.2 shows isorange contours for fixed distance L and some arbitrarily values for ΔT. Plotting the minimum and maximum isoranges for a system is very useful as it gives better visualisation of the system limitations.

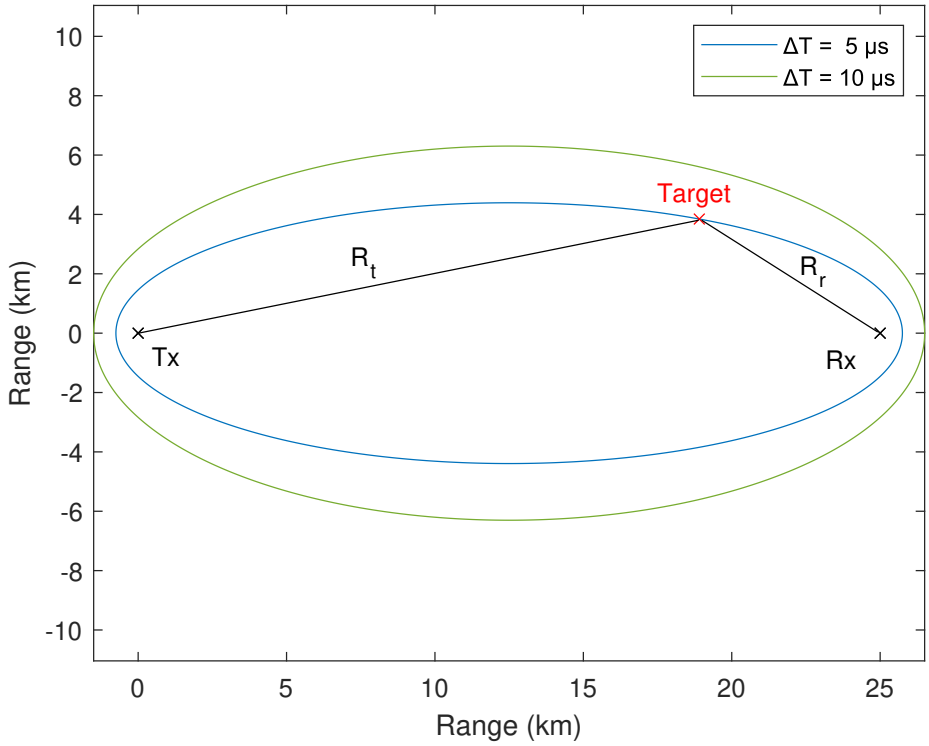

Figure 3.2: Isorange contours for fixed $L = 25$ km.

If the distance L is known and we can measure the time difference ΔT, then we can determine the range sum $R_t + R_r$. However, knowing only L and the range sum is not sufficient to calculate R_r. We still need to know at least one other parameter in the geometry shown in Figure 3.1. If we assume that the angle θ_t is known, then we can write [19]:

$$R_r = \frac{L(e^2 + 1 - 2e\sin\theta_t)}{2e(1 - e\sin\theta_t)} \tag{3.5}$$

Where e is the ellipse eccentricity and is given as:

$$e = \frac{L}{R_t + R_r} \tag{3.6}$$

The angle θ_t is considered to be known since it can be measured. The transmitter antenna is a rotating antenna with a fixed rotation speed. Once the antenna beam is pointing at the receiver, the maximum amount of power is delivered. As the antenna beam is pointing away from the receiver, the received power decreases. Furthermore, we know that after a time duration that corresponds to the antenna rotation speed, the antenna will be pointing again at the receiver. Considering all this we can calculate θ_t.

3.2. Bi-Static Radar Resolution

The range resolution of a bi-static radar is the minimum detectable distance between two targets, that is, the degree to which two targets can be distinguished in range. The two targets are distinguishable in range measurements as long as:

$$\Delta T_2 \geq \Delta T_1 + \tau_c \tag{3.7}$$

Here τ_c is the compressed pulse width. The definition of pulse compression is discussed in Section 4.4. However, if no pulse compression techniques are used, then $\tau_c = \tau$, where τ is the radar pulse duration. From Equation (3.7), an explicit expression for the range resolution ΔR_B can be developed. As shown in Figure 3.3 the bi-static range resolution ΔR_B is defined as the separation between isorange contours. ΔR_B is also called the bi-static range cell. An approximation of ΔR_B is given as:

$$\Delta R_B = \frac{c\tau_c}{2\cos(\beta/2)} \tag{3.8}$$

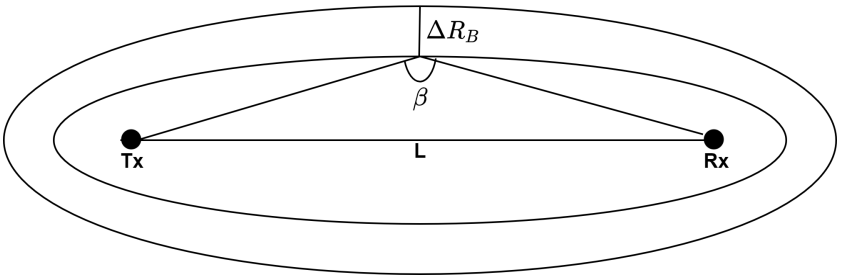

Figure 3.3: Bi-static range resolution.

The derivation of Equation (3.8) is given in [19]. As the target approaches the base line at any point, the bi-static angle approaches $\beta \rightarrow 180°$, the ellipses become more eccentric, $e \rightarrow 1$ (e is defined in Equation (3.6)) and hence $\Delta R_B \rightarrow \infty$. However, the separation between the ellipses cannot approaches infinity anywhere therefore Equation (3.7) is an approximation for the exact separation between the ellipses. Similarly, this is also equivalent for saying that $\Delta T_2 = 0$ in Equation (3.7). Usually, bi-static radar systems are established for a maximum bi-static angle $\beta_{\max}$. Throughout this project $\beta_{\max} = 140°$ is considered. When $\beta_{\max} > 140°$ many approximations used in estimating bi-static radar performance break down. For example, Equation (3.8) breaks down resulting in errors exceeding 45% for all pulse widths and baseline ranges of interest [16].

3.3. Doppler Effect

The Doppler effect is defined as a shift in frequency between the transmitted and received signals. This shift can be caused by the motion of the transmitter, the reflecting object, or the receiver. The Doppler shift is used to measure the radial velocity of the target. Measuring the velocity of the target is not a requirement of the project, however, we provide here a vector based mathematical description of the bi-static Doppler frequency shift as it might be useful for future work.

Since in our case the transmitter, target, and the receiver are moving, we have to take their relative velocities into account. We define the vector $\mathbf{v}$ to be the velocity of the target, $\mathbf{v_r}$ the velocity of the receiver and $\mathbf{v_t}$ the velocity of the transmitter.

The bi-static Doppler shift of the reflected signal from the target can be written as [3]:

$$f_d = \frac{1}{\lambda}\left[\frac{dR_t}{dt} + \frac{dR_r}{dt}\right] \tag{3.9}$$

Where λ is the wavelength. The rate of change of the target to transmitter path dR_t/dt depends on the target and transmitter motion. Therefore, we can write:

$$\frac{dR_t}{dt} = \frac{(\mathbf{v}-\mathbf{v_t})\cdot\mathbf{R_t}}{R_t} \tag{3.10}$$

Where the position $\mathbf{R_t}$ is defined from the target to the transmitter. Similarly, the rate of change of the target to receiver path dR_r/dt depends on the target and receiver motion as:

$$\frac{dR_r}{dt} = \frac{(\mathbf{v}-\mathbf{v_r})\cdot\mathbf{R_r}}{R_r} \tag{3.11}$$

Where the position $\mathbf{R_r}$ is defined from the target to the receiver. Substituting Equations (3.10) and (3.11) in Equation (3.9) yields:

$$f_d = \frac{1}{\lambda}\left[\frac{(\mathbf{v}-\mathbf{v_t})\cdot\mathbf{R_t}}{R_t} + \frac{(\mathbf{v}-\mathbf{v_r})\cdot\mathbf{R_r}}{R_r}\right] \tag{3.12}$$

The Doppler frequency shift f_d given in Equation (3.12) describes the frequency shift of the transmitted signal reflected by the target. However, the direct path signal may also have a frequency shift. The Doppler shift of the direct path signal can be written as:

$$f_{dr} = \frac{1}{\lambda}\left[\frac{dL}{dt}\right] = \frac{1}{\lambda}\frac{(\mathbf{v_r}-\mathbf{v_t})\cdot\mathbf{L}}{L} \tag{3.13}$$

Where the vector $\mathbf{L}$ is defined from the receiver to the transmitter. Finally we can define the relative bi-static Doppler shift f_B, which is the Doppler shift of the reflected signal f_d relative to the Doppler shift of the direct signal f_{dr}:

$$f_B = f_d - f_{dr} \tag{3.14}$$

If we measure the frequency shift between the direct and reflected paths signals f_B and we know the velocities of the receiver and transmitter, then we can calculate the velocity of the target.

3.4. Radar Range Equations

The range equation of the radar can be written in different forms. A description of the parameters given in this section is summarised in Table 3.1. We will start by writing the power received at the receiver site when the transmitter illuminating the receiver assuming an adequate line of sight. The received power due to the direct path can be written according to Friis equation as:

$$P_{rd} = \frac{P_t G_t G_r}{L_s}\left(\frac{\lambda}{4\pi L}\right)^2 \quad \text{(W)} \tag{3.15}$$

When the transmitter is illuminating the target, the power will be intercepted by the target and then will be re-radiated. The re-radiated power will be intercepted at the receiver and is given as:

$$P_r = \frac{P_t G_t G_r \lambda^2 \sigma}{(4\pi)^3 R_t^2 R_r^2 L_s} \quad \text{(W)} \tag{3.16}$$

The derivation of these equation is given in [18]. It is important to mention that the equations do not consider the effects of diffraction, refraction of EM waves neither atmospheric absorption effects. However, for simplicity, we ignore these losses. For the complete equations please refer to [19].
The radar cross section σ expresses the amount of signal power intercepted by that target and scattered in all directions. Equation (3.17) provides a definition of the radar cross section, showing the dependency on the range R_r, and the reflected and incident field strength, E_r and E_i, respectively.

$$\sigma = 4\pi R_r^2 \left|\frac{E_r}{E_i}\right|^2 \tag{3.17}$$

However, from the requirement of this project we consider the radar cross section to be as small as $\sigma = 1\text{m}^2$. L_s accounts for the system losses in both transmitter and receiver chains. The total system losses L_s is usually expressed in dB, since L_s is in the denominator of the radar equation $L_s \geq 0\,\text{dB}$. The peak power P_t is related to the average power as:

$$P_{avg} = P_t \frac{\tau}{PRI} \qquad \text{(W)} \tag{3.18}$$

Table 3.1: Radar equation parameters.

Parameter	Description	Unit
P_t	Peak transmit power	W
G_t	Transmitter antenna gain	-
G_r	Receiver antenna gain	-
G_p	Processing gain	-
L_s	System losses	-
σ	Radar cross section	m^2
λ	Wavelength	m
τ	Pulse duration	s
B	Bandwidth	Hz
PRI	Pulse repetition interval	s
SNR	Signal to noise ratio	-
F	Noise factor	-

The target detection process is based on the echo from a single pulse. We can detect a target as long as the received power P_r is above a certain threshold of the noise power P_n at the receiver. The noise power is expressed in Equation (3.19):

$$P_n = k_b T_0 B F \qquad \text{(W)} \tag{3.19}$$

Where k_b is Boltzmann's constant, $k_b = 1.38 \times 10^{-23}\,\text{JK}^{-1}$. $T_0 = 290\,\text{K}$ is the ambient temperature. B is the receiver bandwidth. F is the noise factor ($F > 1$). The noise figure NF is the noise factor but given in dB $NF = 10\log(F)$. The noise figure/factor must account for all noise added in the receiver chain (SDR, PA, BPF, mixer, etc.).
We can write Equation (3.16) in terms of signal to noise ratio SNR $= P_r / P_n$. This yields:

$$\text{SNR} = \frac{P_t G_t G_r \lambda^2 \sigma}{(4\pi)^3 R_t^2 R_r^2 L_s k_b T_0 B F} G_p \tag{3.20}$$

G_p is the processing gain due to pulse compression and matched filtering, both are discussed in the Chapter 4. The processing gain G_p is computed as:

$$G_t = B\tau \tag{3.21}$$

For a minimum SNR we can define a maximum detectable range product and rewrite Equation (3.20) as:

$$(R_t R_r)_{\max} = \left(\frac{P_t G_t G_r \lambda^2 \sigma}{(4\pi)^3 L_s k_b T_0 B F (\text{SNR})_{\min}} G_p \right)^{\frac{1}{2}} \tag{3.22}$$

$(R_t R_r)_{\max}$ in Equation (3.22) illustrates maximum range corresponding to the same SNR value as shown by the oval of Cassini. The ovals of Cassini are discussed in Section 3.5. Equation (3.20) is useful to plot ovals of Cassini as a function of the available SNR.

Usually, in radar systems the minimum SNR required for detection is established based on desired false alarm and detection probabilities. There are different models that describe theses probabilities and their relation to the SNR. Here, we consider the Swerling-1 model which assumes a constant radar cross section during processing interval. The SNR is related to probability of false alarm P_{FA} and probability of detection P_D as:

$$\text{SNR} = \frac{\log(P_{FA})}{\log(P_D)} - 1 \tag{3.23}$$

3.5. Ovals of Cassini

A Cassini oval is defined as a curve such that for any point on the curve the product of two distances to two fixed points is constant. Cassini ovals can also be considered as contours of constant 'range' and power [8], 'range' is referring here to the product $R_t R_r$. Applying this to the geometry shown in Figure 3.1, we can construct curves as a function of SNR where $R_t \times R_r$ is constant for a fixed length L. In polar form, a Cassini oval equation is given as:

$$r^4 - 2a^2 r^2 \cos(2\theta) = b^4 - a^4 \tag{3.24}$$

Equation (3.20) can be rewritten as:

$$R_t^2 R_r^2 = \frac{P_t G_t G_r G_p \lambda^2 \sigma_t}{(4\pi)^3 L_s k_b T_0 B F} \frac{1}{\text{SNR}} \tag{3.25}$$

If we consider the first fraction to be constant K, we can plot the $R_t^2 R_r^2$ as a function of SNR:

$$R_t^2 R_r^2 = \frac{K}{\text{SNR}} \tag{3.26}$$

By writing R_t and R_r in polar form, we conclude that the SNR contours are defined by ovals of Cassini with:

$$\begin{aligned} a &= \frac{L}{2} \\ b &= \left(\frac{K}{\text{SNR}}\right)^{\frac{1}{4}} \end{aligned} \tag{3.27}$$

Figure 3.4 shows ovals of Cassini for different SNR and K arbitrarily set to $K = 30L^4$. At each point on a Cassini oval for a given SNR, the product $R_t \times R_r$ is constant. As we can see from the figure, the SNR decreases as the range product increases. Ovals of Cassini plot is very useful in radar system design as it gives a better visualisation of the power limited region and system limitations. It should be noted that Figure 3.4 is merely for the sake of illustration.

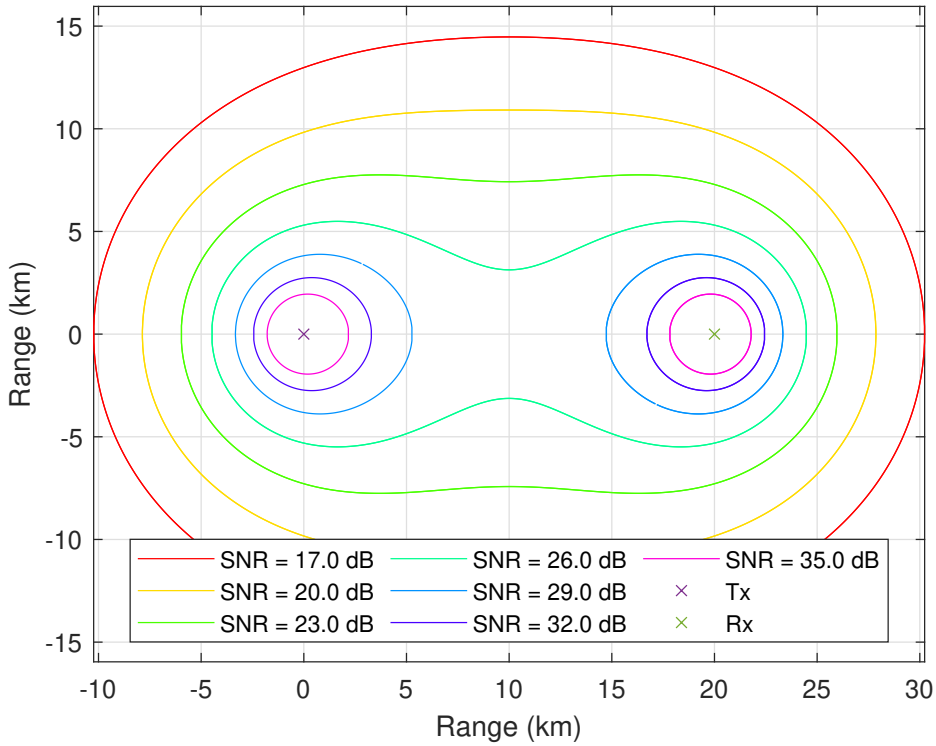

Figure 3.4: Ovals of Cassini – Transmitter is at the origin and receiver is located at 20 km at the x-axis.

4

Waveform Design

4.1. Introduction to Radar Waveforms

Since the invention of radar, many radar waveforms have been developed. Each waveform has its properties, advantages and disadvantages. Depending on the application, the one waveform preforms better than the other. Radar waveforms can be classified in two categories, continuous waveforms and pulsed waveforms. Within each category, different waveforms can be distinguished based on the modulation. However, continuous waveforms such as Frequency Modulated Continuous Waveform, FMCW for short, requires clock synchronisation of transmitter and receiver clocks. FMCW requires an additional antenna at the receiver that is aimed at the transmitter antenna. Therefore, we are only considering pulsed waveforms.

The waveform design is very important in radar systems. The radar waveform is responsible for the accuracy, resolution, and ambiguity of measurements.
The collective features of a pulsed radar waveform are:

1. Carrier frequency f_c (Hz).
2. Pulse width τ (s).
3. Pulse repetition frequency f_p (Hz) or the pulse repetition interval $PRI = \frac{1}{f_p}$ (s).
4. Modulation within the pulses.

The first three features are illustrated in Figure 4.1

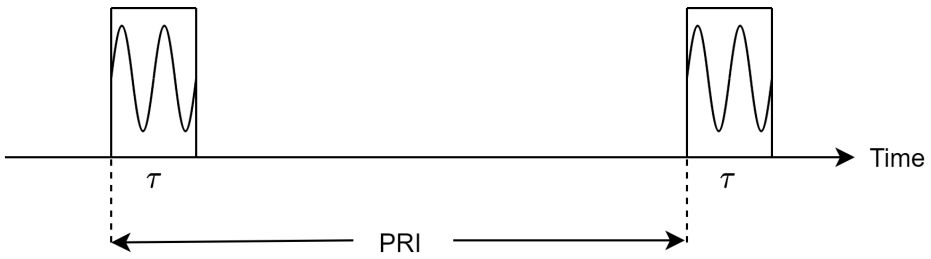

Figure 4.1: Train of transmitted pulses.

The transmitter continuously transmits a train of RF pulses. The receiver antenna receives the pulses from the direct path and reflected pulses from the target. We have to ensure that the echo of a target, located within the range requirements of the project, is received before the transmission of the next pulse. If we assume that the pulse width τ is much smaller than the pulse repetition period PRI, we can determine the repetition frequency f_p:

$$f_p = \frac{c}{(R_t + R_r)_{max}} \tag{4.1}$$

The range resolution of the radar can be improved by using short pulses as can be deduced from Equation (3.8) in Chapter 3. However, utilising short pulses decreases the transmitted power as seen in the radar equation. Since the transmitted power is directly proportional to the receiver SNR, it is desirable to increase the pulse width while maintaining adequate range resolution. This can be done by means of a pulse compression techniques that allow us to transmit long pulses while obtaining range resolution corresponding to a short pulse. In addition to pulse compression, matched filtering is usually applied to the received signal to maximise SNR and achieve a processing gain. In this chapter, we start by providing a mathematical description of the radar signals. Thereafter, we discuss matched filtering, pulse compression and windowing.

4.2. Representation of Radar Waveforms

The majority of radar signals are narrow bandpass signals. A narrow bandpass signal can be written in several forms. One form is given as [4]:

$$s(t) = g(t)\cos[2\pi f_c t + \phi(t)] \tag{4.2}$$

Where $g(t)$ is the envelope of $s(t)$ and $\phi(t)$ is the instantaneous phase. Although, signals in physical systems are real, it is mathematically convenient to describe the signal in a complex representation:

$$s(t) = Re\left[g(t)e^{j(\omega_c t+\phi(t))}\right] = \Re[z(t)] \tag{4.3}$$

Where $s(t)$ is the projection of the rotating phasor signal $z(t)$ (rotating CCW in the real-imaginary plane) on the real axis. We can also describe the signal as:

$$s(t) = \frac{1}{2}\left[z(t) + z^*(t)\right] \tag{4.4}$$

Where the signal is represented as a sum of two complex phasors. One rotating CCW (positive frequency) and the other CW (negative frequency) in the real-imaginary plane. The signal representation in Equation (4.3) has single sided spectrum while the representation given in Equation (4.4) results in double sided spectrum with even symmetry about the origin.
Since all Software Defined Radio devices utilise I-Q mixers as shown in Figure 4.2, it is convenient to represent the signal in I-Q components:

$$s(t) = g_c(t)\cos(\omega_c t) - g_s(t)\sin(\omega_c t) \tag{4.5}$$

Where $g_c(t)$ is the in-phase component and $g_s(t)$ is the quadrature component and they are given by:

$$g_c(t) = g(t)\cos(\phi t) \tag{4.6}$$

$$g_s(t) = g(t)\sin(\phi t) \tag{4.7}$$

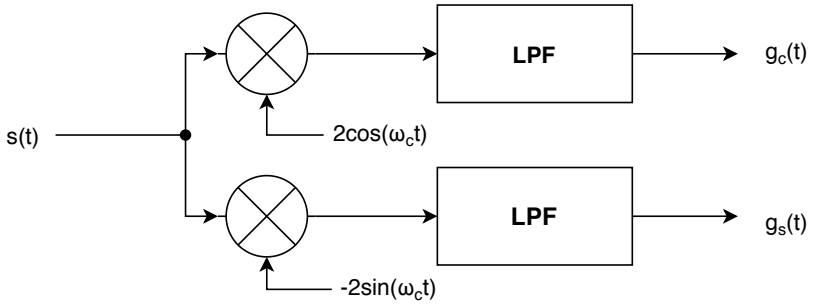

Figure 4.2: A block diagram of a I-Q detector.

From the I-Q components of the signal we can define the complex envelope $u(t)$:

$$u(t) = g_c(t) + jg_s(t) \tag{4.8}$$

With the complex envelope we can write the signal as:

$$s(t) = \Re\left[u(t)e^{j\omega_c t}\right] \tag{4.9}$$

Note that:

$$g(t) = |u(t)| \tag{4.10}$$

4.3. Matched Filter

The matched filter is needed to maximise the SNR of the received signal. The matched filter concentrates the entire energy of the signal into an output peak at a predetermined additional delay t_0, hence improving the signal-to-noise ratio.

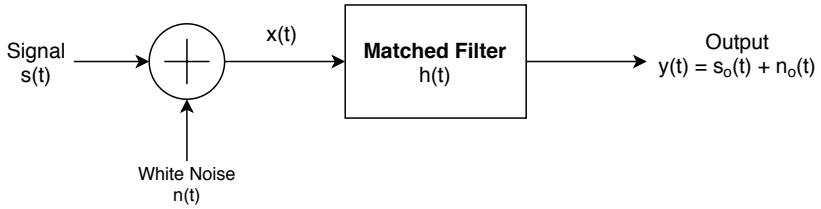

Figure 4.3: A bock diagram of a matched filter.

Consider the block diagram shown in Figure 4.3, the input to matched filter is the signal $s(t)$ added with white Gaussian noise $n(t)$. The impulse response $h(t)$ or the transfer function $H(\omega)$ that will yield maximum output signal-to-noise ratio at a predetermined delay t_0 are given in the following equations [11]:

$$H(\omega) = S^*(\omega)\exp(-j\omega t_0) \tag{4.11}$$

$$h(t) = s^*(t_0 - t) \tag{4.12}$$

As stated in Equation (4.12), $h(t)$ is is a delayed mirror image of the conjugate of the signal. The output of the matched filter without noise is given as:

$$s_o(t') = \int_{-\infty}^{\infty} s(\alpha)s^*(\alpha - t')\,\mathrm{d}\alpha \tag{4.13}$$

Where $t' = t - t_0$ and α is a dummy variable for integration. Equation (4.13) is the autocorrelation function of $s(t)$ where it is delayed to have a maximum peak at time t_0. In the presence of noise $n(t)$, the output of the matched filter is given by:

$$y(t) = x(t) * s^*(t_0 - t) \tag{4.14}$$

Without the presence of noise, the output of the matched filter for narrow band signals can be approximated to the following [19]:

$$s_0(t) = Re\left[u_0(t)e^{j\omega_c t}\right] \tag{4.15}$$

Where $u_0(t)$ corresponds to the matched filter output of the complex envelope $u(t)$ of the signal $s(t)$ for $t_0 = 0$:

$$u_o(t) = \int_{-\infty}^{\infty} u(\alpha)u^*(\alpha - t)\,\mathrm{d}\alpha \tag{4.16}$$

Therefore, it is convenient to only consider the complex envelope $u(t)$ of the narrow band signal as stated in Equation (4.15).

4.4. Pulse Compression

The bandwidth B of unmodulated pulse (real pulse whose spectrum is centred in the baseband) is defined at -3 dB spectrum width which is equal to $1/\tau$. Waveform properties are defined in terms of matched filter response. A general output of the matched filter is shown in Figure 4.4 The first null happens at $1/B$. For unmodulated pulses this is equal to τ, hence the mainlobe width is 2τ. However, the sidelobes do not exists for unmodulated pulses. Our goal is to reduce the mainlobe width to obtain good range resolution without reducing the pulse duration τ. Radar range resolution is governed by the width of the mainlobe. Two targets are considered to be distinguished in range if the mainlobe peak of one target falls on the first null of the second target. This means the two peaks must be at least separated by τ. This is not always true. In some cases, when the amplitude of one peak is much higher than the other peak or there is a phase shift between the two received pulses, it will not be possible to distinguish the two peaks with a separation of τ as this may require

longer separation. However, for simplicity, throughout this project we consider τ as a minimum separation distance between two peaks.

Reducing the width of the sidelobes without shortening the pulse duration can be done by pulse compression. However, as a result of pulse compression, the sidelobes are introduced. Sidelobes are undesirable and problematic because sidelobes associated with high amplitude signals may suppress the mainlobe peak of low amplitude signals. Sidelobe performance is defined as *peak sidelobe ratio* which is the ratio of the main peak to the peak of the sidelobe. The sidelobes can be reduced by means of windowing. However, windowing will introduce some losses and will generally increase the mainlobe width.

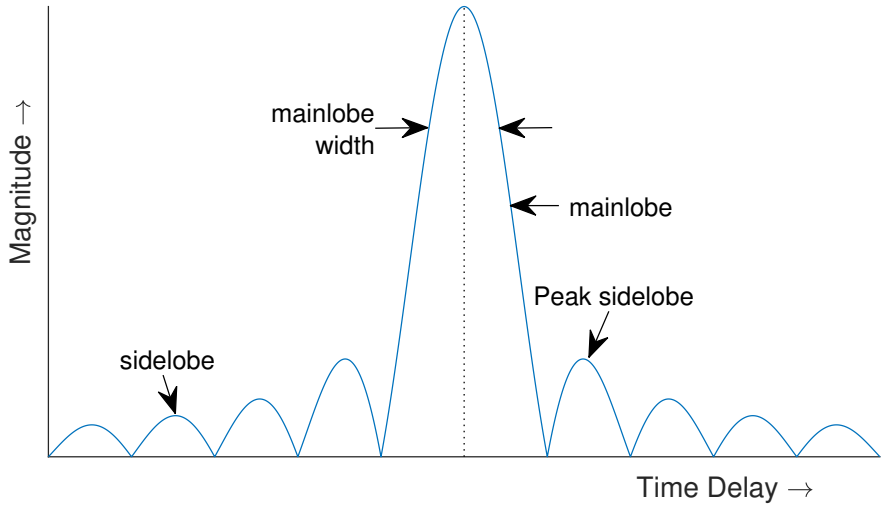

Figure 4.4: General response of matched filter

In the following sections, we examine different pulse compression waveforms and eventually provide a choice for the most suitable waveform for our project. Thereafter we discuss the concept of windowing.

4.4.1. Pulse Compression Waveforms

The idea behind pulse compression is to decouple the energy and resolution by means of phase or frequency modulation such that $B >> 1/\tau$. Phase-coded waveforms can be designed to achieve a perfect narrow mainlobe width and very low sidelobe response. However, Phase-coded waveforms are not Doppler tolerant. When there is a frequency mismatch between the received signal and the matched signal, the mainlobe peak disappears and the target is not detectable anymore. This problem can be solved by using two-dimensional matched filtering which matches the received signal with possible frequency shifted versions of the transmitted signal. However, this is very computationally intensive, therefore we avoid using this waveform.

Frequency modulation waveform refers to changing the frequency of the signal during its pulse duration. This can be done by varying the frequency either linearly or non-linearly. Linear frequency modulation (LFM) is the most popular pulse compression method. LFM waveform is Doppler tolerant. Having a frequency mismatch will not cause mainlobe peak to disappear. Since, the mother-ship, target and receiver are all in motion, we will have Doppler frequency shift. Therefore, LFM waveform is very suitable for our project. The properties of LFM are discussed in detail in Section 4.4.2, however one disadvantage of LFM is high peak to sidelobe ratio. Nevertheless, this can be resolved by using amplitude weighting window.

Applying pulse compression introduces a gain in SNR at the output matched filter. This is called *pulse compression gain* G_p which is defined as the ratio of SNR at the output of the matched filter to the SNR at the input of the matched filter. The pulse compression gain is included in the radar equation (see Equation (3.20)) and is defined as the time-bandwidth product $G_p = B\tau$.

4.4.2. Linear Frequency Modulated Waveform

Linear Frequency Modulated Waveform is also called a chirp or simply LFM for short. The waveform can be described as sinusoid whose frequency is linearly changing with time [14]. The frequency sweep of an LFM waveform can go either up or down. A real baseband LFM waveform as seen in Figure 4.5 is expressed in Equation (4.17) with B (Hz) is the sweep bandwidth of the frequency modulation and τ (s) is the pulse width. The waveform can also be expressed in the complex form and even in bandpass, Equation (4.18) expresses the complex waveform in bandpass with f_0 is the carrier frequency. As can be seen from Figure 4.5 and as indicated by the '+' sign in Equations (4.17) and (4.18) the frequency sweep is in upward direction.

$$x(t) = A\cos\left(\pi\frac{B}{\tau}t^2\right) \tag{4.17}$$

$$x_{bp}(t) = A\exp\left(2\pi f_0 t + \pi\frac{B}{\tau}t^2\right) \tag{4.18}$$

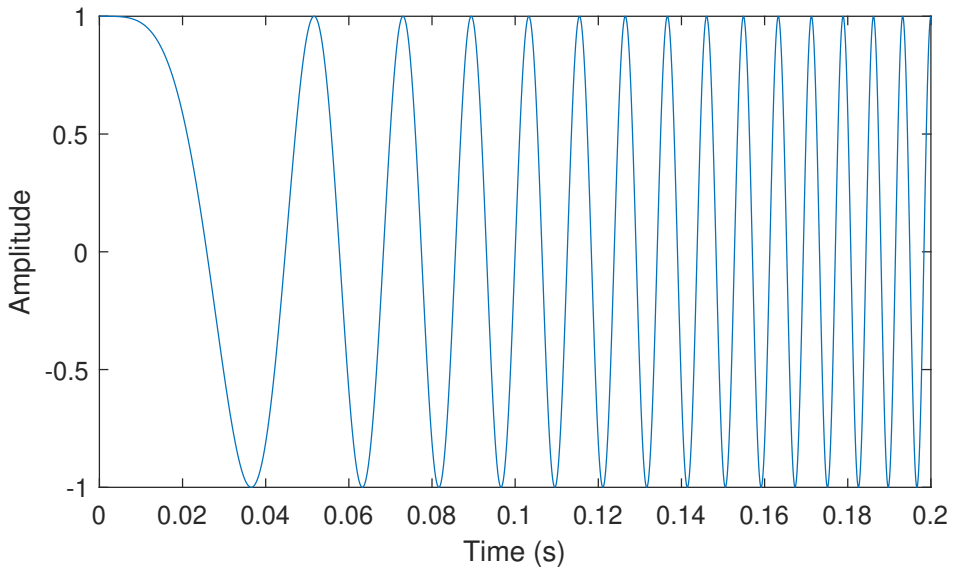

Figure 4.5: An example of a baseband LFM waveform in time domain with $0 \leq t \leq \tau$, $B = 150\,\text{Hz}$ and $\tau = 200\,\text{ms}$.

The linear frequency modulation is proved by differentiating the instantaneous phase of the waveform. The first time derivative of the instantaneous phase shows that the instantaneous frequency in radians per second, is increased at a rate of B/τ as time progresses (Equation (4.19)).

$$\frac{d}{dt}\phi(t) = \frac{d}{dt}\left(\pi\frac{B}{\tau}t^2\right) = 2\pi\frac{B}{\tau}t \tag{4.19}$$

And the instantaneous frequency in hertz is:

$$f(t) = \frac{B}{\tau}t \tag{4.20}$$

LFM waveforms have some interesting characteristics that are very useful. One of the advantages of LFM waveforms is the energy they contain. As the time-bandwidth product $\tau \cdot B$ increases, LFM waveforms show some resemblance to square waves. For $\tau B > 100$ the waveform contains approximately 98% to 99% of the energy [14], unlike a pure sinusoid for instance. Moreover, LFM waveforms are known to have excellent Doppler tolerance [7]. This refers to the fact that LFM waveforms exhibit range-Doppler coupling and a preservation of the mainlobe and sidelobe response over large fractional Doppler shifts. Based on the equations of the matched filter provided in Section 4.3 and the mathematical representation of and LFM waveform in Equation (4.18), we can find the response of the matched filter when matched to the LFM waveform. The result is as follows [14]:

$$y(t) = \left(1 - \frac{|t|}{\tau}\right)\left(\frac{\sin\left[\left(1 - \frac{|t|}{\tau}\right)\pi B t\right]}{\left(1 - \frac{|t|}{\tau}\right)\pi B t}\right) \qquad |t| \leq \tau \tag{4.21}$$

The response can be approximated in the vicinity of the mainlobe peak ($t << \tau$) as [14]:

$$y(t) = \left(1 - \frac{|t|}{\tau}\right)\left(\frac{\sin(\pi B t)}{\pi B t}\right) \qquad |t| \leq \tau \tag{4.22}$$

From Equation (4.22), we can find the first zero crossings of the response. This occurs when:

$$t = \pm\frac{1}{B} \tag{4.23}$$

This equation shows clearly the advantages of pulse compression. As seen earlier, with unmodulated pulses ($B\tau = 1$), the first null occurs at $t = \tau$. However, with LFM we can decrease the mainlobe width by increasing the bandwidth while maintaining an adequate pulse duration τ for the SNR. As discussed earlier, two targets are distinguishable in range as long as the two peaks are separated by τ. However, after pulse compression, this separation refers to the first null of the matched filter response. To avoid ambiguity, we call this separation as *compressed pulse width* (symbol τ_c).

Figure 4.6 shows an example response of LFM matched filter with time bandwidth product $\tau B = 4000$. The peak to sidelobe ratio is -13.3 dB and the first null occurring at $1/B \approx 0.05\,\mu$s .

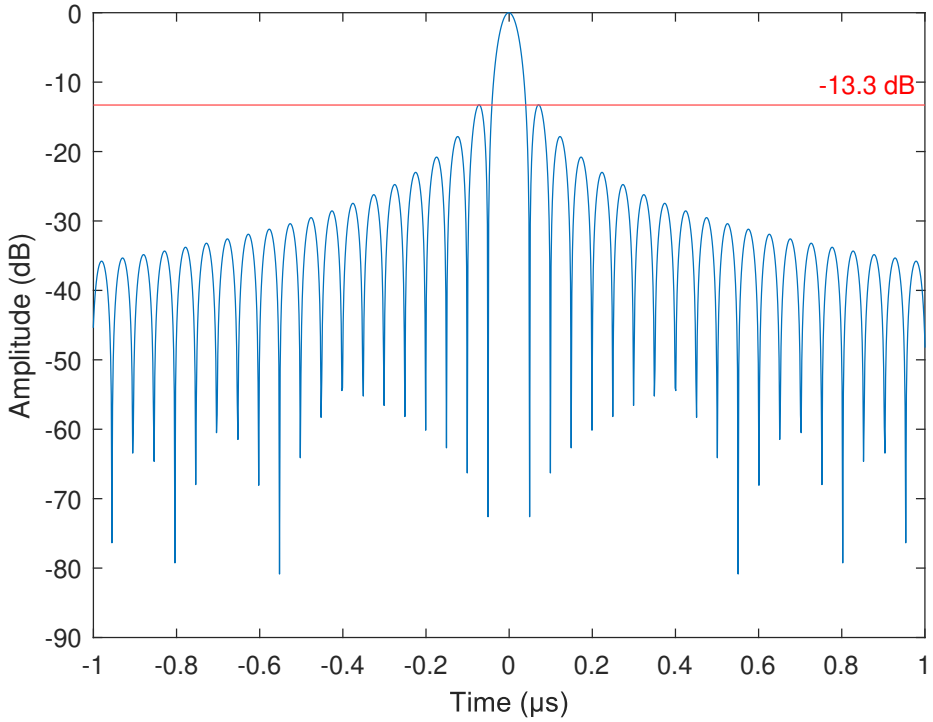

Figure 4.6: Matched filter response for LFM waveform with $B = 20$ MHz and $\tau = 200\,\mu$s. The figure is limited between -1 and $1\,\mu$s.

So far, we have assumed that there is no mismatch between the matched filter and the signal received. However, as discussed in Chapter 3, there might be Doppler frequency shift between the transmitted and the received signal. This mismatch will change the response of the matched filter. Without the exact knowledge of the Doppler shift, the radar receiver cannot modify its matched filter to the new frequency and hence mismatch occurs. A very useful mathematical tool called *ambiguity function* describes the response of the

matched filter when the input signal is Doppler shifted by f_d relative to nominal value (zero) for which the matched filter was designed. The ambiguity function is expressed as [14]:

$$\chi(t, f_d) = \left| \int_{-\infty}^{\infty} u(\alpha) e^{j2\pi f_d \alpha} u^*(\alpha - t) \mathrm{d}\alpha \right| \tag{4.24}$$

For zero Doppler shift $f_d = 0$, the ambiguity function is equal to the magnitude matched filter response. The ambiguity function achieves its maximum at zero delay and zero Doppler. More information about the ambiguity function can be found in [11]. The ambiguity function for LFM can be written as [14]:

$$\chi(t, f_d) = \left| \left(1 - \frac{|t|}{\tau}\right) \left(\frac{\sin\left[\pi t \left(1 - \frac{|t|}{\tau}\right)\left(f_d + \frac{B}{\tau} t\right)\right]}{\pi t \left(1 - \frac{|t|}{\tau}\right)\left(f_d + \frac{B}{\tau} t\right)} \right) \right| \quad |t| \leq \tau \tag{4.25}$$

We can deduce from Equation (4.25) that when there is a Doppler shift f_d, the peak of the matched filter response will be attenuated and shifted in time. The time shift amount corresponds to $-f_d \frac{\tau}{B}$ and the attenuation will be caused due to $\left(1 - \frac{|t|}{\tau}\right)$. An example of matched filter response with $f_d = 0$ and $f_d = 4\,\mathrm{kHz}$ is shown in Figure 4.7. As we can see for Doppler shift of 4 kHz the peak is shifted with 0.04 µs. This little shift will cause the target to appear farther compared to its actual location. However, this is not problematic as the range error is very small. The inaccuracy of range measurement is discussed in Chapter 6.

The effects of Doppler shift can also be examined in frequency domain. The frequency mismatch between the matched filter and the Doppler shifted waveform results a composite spectrum with reduced bandwidth that approximately equals to $B - |f_d|$ [14]. This reduction in the bandwidth, reduces the range resolution. However, this will be too small and negligible as discussed in Chapter 6.

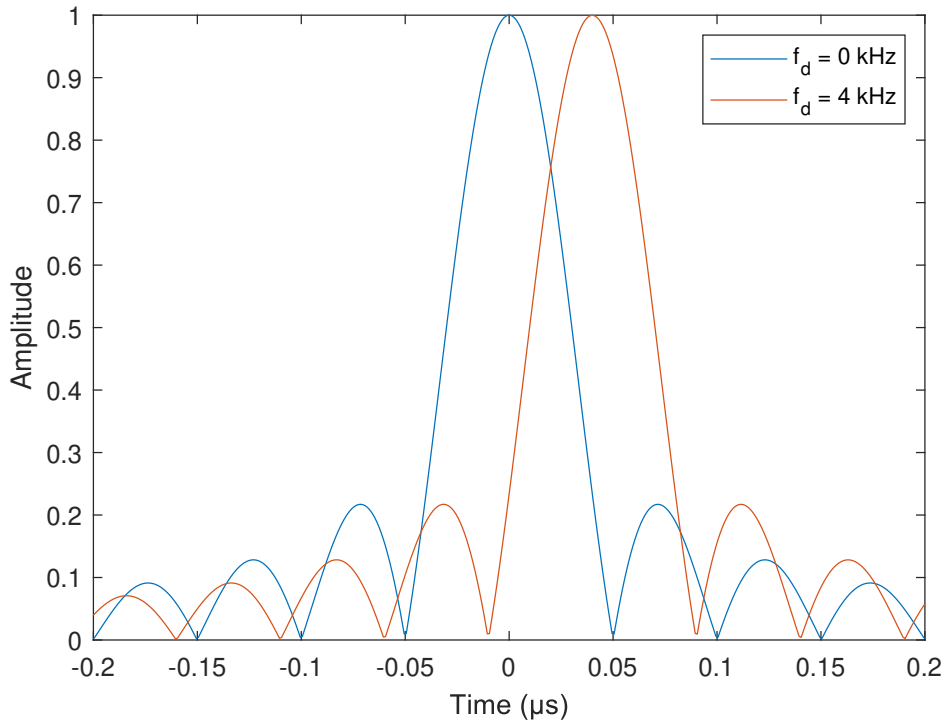

Figure 4.7: Matched filter response of an LFM waveform with $B = 20\,\mathrm{MHz}$ and $\tau = 200\,\mu\mathrm{s}$ for 0 and 4 kHz Doppler shift.

4.5. Windowing

For LFM waveform with time bandwidth product $B\tau > 40$ has peak sidelobe ratio of −13.5 dB [11]. As stated earlier, sidelobes are problematic as they may suppress the presence of echoes with low energy and hence

degrade the performance of the system. The peak sidelobe ratio can be reduced by windowing functions. However, windowing functions slightly increase the mainlobe width and introduce losses. The LFM peak sidelobe ratio (−13.5 dB) is usually unacceptable in radar systems. Windowing the LFM waveform, for which the matched filter is matched to, is the most common method to reduce the peak to sidelobe ratio. Windowing is done by multiplying the waveform with a mathematical function that is zero-valued outside some chosen interval. The analysis provided in the previous sections assumes a rectangular window. The rectangular window is a multiplication of the waveform with 1 during the pulse duration and zero outside this interval. There are many different window functions. Here, we consider two window functions: *Hamming* and *Blackman-Harris* window functions and compare them to the rectangular window.

Hamming window is defined as [2]:

$$w_B(t) = \begin{cases} 0.54 - 0.46\cos\left(2\pi\frac{t}{\tau}\right) & 0 \le t \le \tau \\ 0 & \text{otherwise} \end{cases} \tag{4.26}$$

A four-term Blackman-Harris window is given as [2]:

$$w_B(t) = \begin{cases} 0.36 - 0.49\cos\left(2\pi\frac{t}{\tau}\right) + 0.14\cos\left(4\pi\frac{t}{\tau}\right) - 0.01\cos\left(6\pi\frac{t}{\tau}\right) & 0 \le t \le \tau \\ 0 & \text{otherwise} \end{cases} \tag{4.27}$$

Figure 4.8 shows the response of the matched filter for LFM waveform with employing rectangular, Hamming, and Blackman-Harris window functions. Figure 4.9 shows the response zoomed in between $-1 \le t \le 1\,\mu$s. In Table 4.1 a comparison has been made between the window functions. The peak side-lobe ratios shown in table 4.1 for Hamming and Blackman-Harris windows, are only achieved for $B\tau > 200$.

Hamming window reduces the peak to sidelobe by −28.2 dB relative to rectangular window. However, this comes with a penalty. Hamming window introduces losses of −5.6 dB and increases the compressed pulse width by a factor of 2 and hence, decreases the range resolution by a factor of 2.

Blackman-Harris window provides more improvement in peak to sidelobe ratio as this is decreases by −78.5 dB relative to the rectangular window. Nevertheless, the range resolution is degraded by a factor of 4 and the peak gain losses are increase to −9 dB relative to rectangular window.
In Appendix A.3 and A.4 a MATLAB function has been made to implement matched filtering and windowing with a script to generate LFM waveform and plot the response.

Table 4.1: Properties of window functions.

Window	Peak gain (dB) relative to rectangular window peak	Compressed pulse width	Peak to sidelobe ratio (dB)
Rectangle	0.0	1/B	-13.5
Hamming	-5.6	2/B	-41.7
Blackman-Harris	-9.0	4/B	-92.0

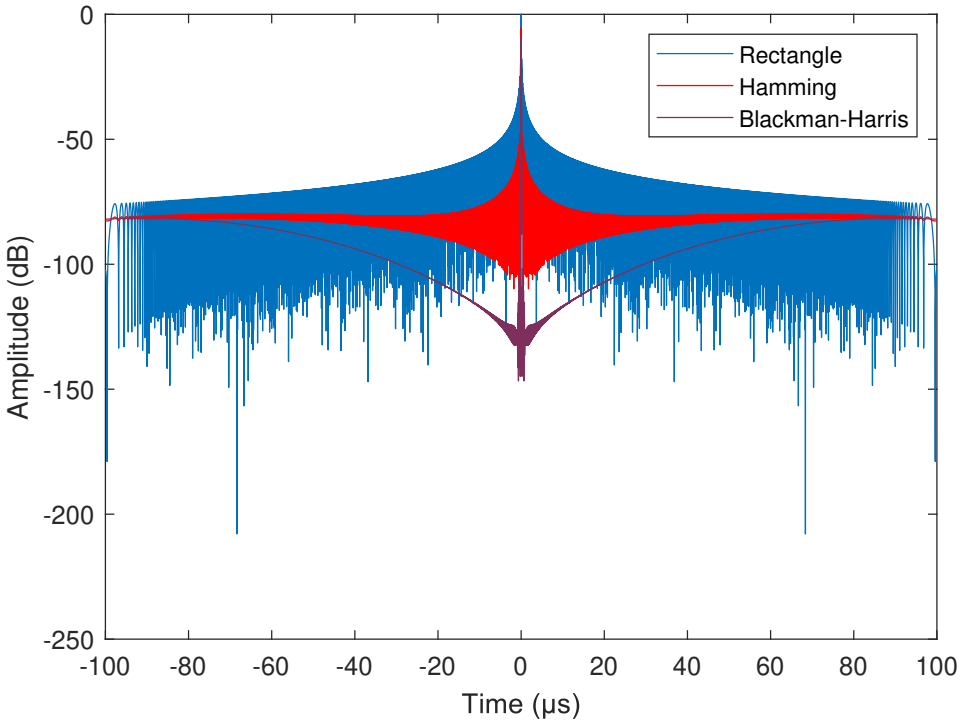

Figure 4.8: Matched filter response for different windows applied to an LFM waveform with $B = 20\,\text{MHz}$ and $\tau = 200\,\mu\text{s}$.

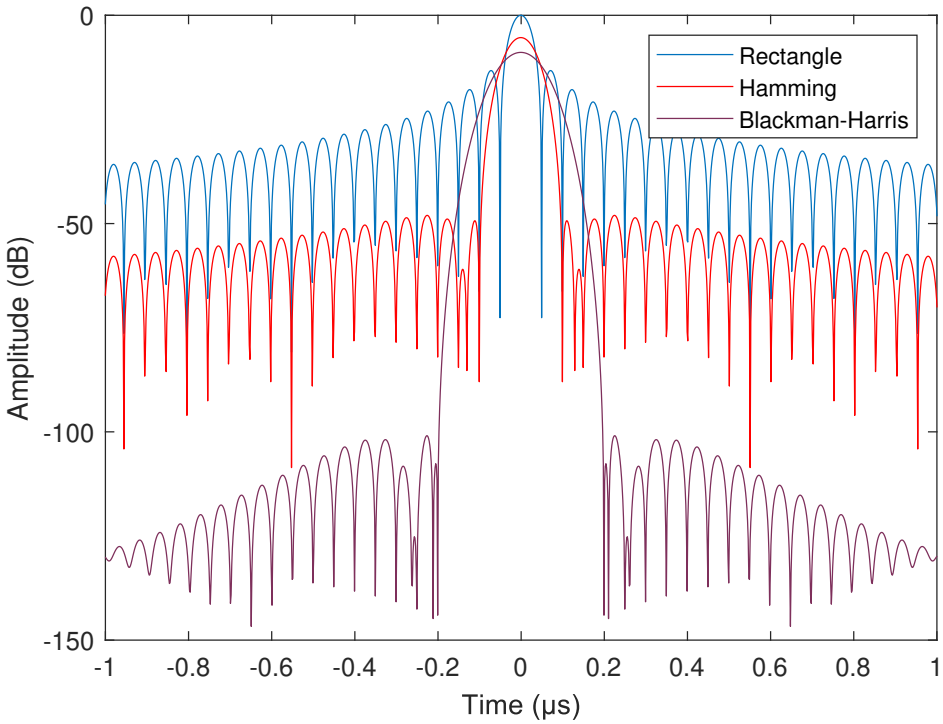

Figure 4.9: Matched filter response for different windows applied to an LFM waveform with $B = 20\,\text{MHz}$ and $\tau = 200\,\mu\text{s}$. Figure 4.8 for $-1 \leq t \leq 1\,\mu\text{s}$.

5

System Overview and Software Defined Radio

The goal of the project is to design a bi-static radar system that is capable of measuring the radial distance of a target from the receiver. The system should be implemented within Software Defined Radio (SDR). Software Defined Radio is a device in which some or all of the physical layer functions are software defined. At the time of writing this thesis, many shapes and sizes of SDRs are available in the market. Such a device has an architecture that typically includes processors—whether that is on board or on the computer—FPGAs and RF front ends. For the sake of formality, the following definition is stated.

Definition of Software Defined Radio:
An SDR is defined as a radio in which the receive digitisation is performed at some stage downstream from the antenna, typically after wide-band filtering, low noise amplification, and down conversion to a lower frequency in subsequent stages – with a reverse process occurring for the transmit digitisation. Digital signal processing in flexible and reconfigurable functional blocks defines the characteristics of the radio [17].

5.1. Software Defined Radio for Radar Applications

The role of the Software Defined Radio within the BiSAD is to implement the waveform generator in the transmitter chain and implement the signal processor in the twin-receiver chain as depicted in Figure 5.1. Ideally, the Software Module is implemented on SDR, subsequently eliminating the Host PC. As a matter of fact, it possible to design a system with standalone SDRs making the system compact and flexible. Nonetheless, for the time being simple and affordable SDRs—that need a host PC—are used in this project.

The frequency band in which the radar system will transmit and receive is a design choice that should be tackled in early design stages. The Dutch regulatory body of the radio spectrum Agentschap Telecom provides a chart with a clear overview of the radio spectrum. Taking into account the open frequencies according to this chart and the licenses that the Delft University of Technology has in its repository, the options are narrowed down to S-band and X-band. The S-band is defined as the frequency range 2–4 GHz. This band has a license free frequency range of 2.4–2.5 GHz, whose typical applications include Wi-Fi, Bluetooth and ZigBee. The X-band is defined as the frequency range 8–12 GHz and has a license free frequency range 9.2–10 GHz.

The two possible frequency ranges translate to the following in terms of wavelengths: 11.99 up to 12.49 cm for S-band and 3.00 up to 3.26 cm for X-band. The choice of the one option over the other affects the range resolution, signal attenuation due the atmosphere e.g. due to particles in the air or rain drops, and the size of the antennas. Comparing the S-band and X-band based on range resolution, atmospheric attenuation and antenna size, X-band seems to be the better choice due to the smaller antenna size and the better range resolution, despite the worse the attenuation. The antenna size not only means a bulky system, it also means more expensive equipment. Since there is a large restriction on the weight and the size of the systems, mainly on the antennas, and the receiver system requires two antennas in vertical orientation while having limited space to work, again X-band seems optimal.

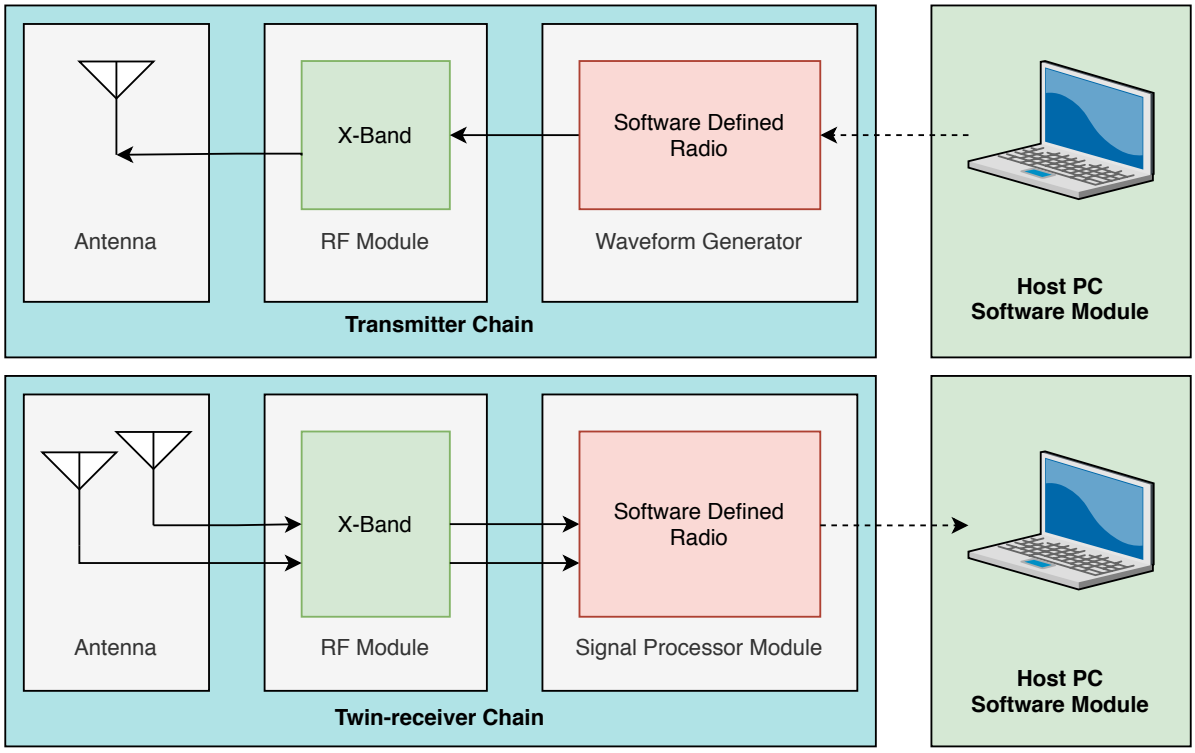

Figure 5.1: A diagram illustrating a high-level representation of BiSAD.

Beside choosing the operating frequency band, the centre frequency should be determined. The centre frequency should lie between the licensed license free frequency range 9.2–10 GHz. Depending on the transmitter and receiver antennas, the chosen centre frequency is $F_c = 9.7\,\text{GHz}$.

5.2. Selection of Software Defined Radio

For the selection of an SDR, attention should be paid to the signals it will handle. The RF stage of design is located in the X-band. At the time of writing this thesis, the majority of the SDRs with affordable prices operate up to 6 GHz. In order to keep the design affordable, an RF front end is designed instead of picking a expensive SDR suitable for X-band. This implies that an up converter is needed in the transmitter chain which converts the centre frequency of the waveform to the desired one. The up conversion is done by mixing the waveform with a local oscillator. The SDR should provide both the waveform and the local oscillator signals. Similarly, at the receiver site, the SDR should provide a local oscillator signal to down convert the frequency to the desired one. In addition, the receiver SDR should provide dual receive channel for the twin-antennas.

Therefore, the number of channels supported by the SDR is an important parameter to consider. The optimal choice here would be a dual transmit channel SDR that can be programmed to transmit the radar waveform through one channel and a pure sinusoid that can be used as a local oscillator in the RF front end through the other. Similarly, the receiver SDR must provide two receive channels and one transmit channel for the local oscillator. The frequency range of the SDR should include the local oscillator and the IF frequency listed in Table 5.1. Furthermore the sampling rates of the ADC/DAC in the SDR should adhere to the Nyquist Sampling Theorem – see Equation (5.1). As discussed in Chapter 4, increasing the bandwidth of the waveform, improves the range resolution of the radar. Therefore, our aim is to use the maximum available bandwidth of the SDR.

$$2 \cdot B \leq F_s \tag{5.1}$$

The USRP B210 by Ettus Research (see Figure 5.2) is selected for this project. This device costs €1,290.00 on

the official website of the Ettus Research (www.ettus.com) and has some interesting features that are useful for this project. A high-level diagram illustrating the components of this SDR is provided in Figure 5.3. Ettus Research offers a variety of SDRs that have many features in common, therefore only a general schematic of the architecture is provided. Figure 5.4 provides the general architecture.
Some interesting features of the USRP B210 are:

- RF coverage from 70 MHz – 6 GHz
- Flexible rate 12-bit ADC/DAC
- 2 TX & 2 RX, Half or Full Duplex
- Fully-coherent 2x2 MIMO capability
- Up to 30.72 MHz of instantaneous bandwidth in 2x2
- Includes DC power supply
- GPIO capability

Table 5.1: Parameters to considering for SDR selection.

Parameter	**Symbol**	**Value**	**Unit**
Centre frequency	f_c	9.7	GHz
Local oscillator	f_{lo}	5.825	GHz
Intermediate frequency	f_{if}	3.875	GHz

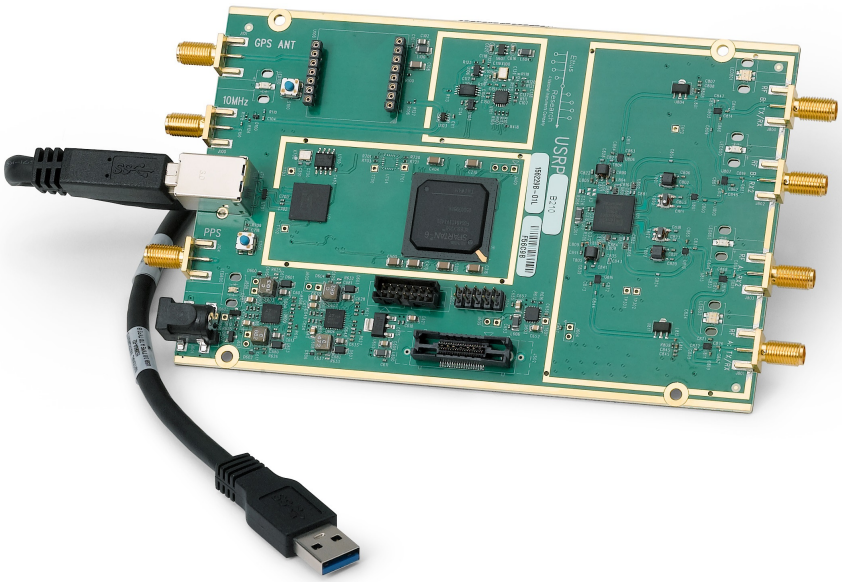

Figure 5.2: The USRP B210 (image courtesy of Ettus Research).

In general, USRP hardware—as presented in Figure 5.4—implements a direct conversion analogue front end with analogue-to-digital converters (ADCs) and digital-to-analogue converters (DACs) featuring an FPGA for the digital down conversion (DDC) and digital up conversion (DUC) steps. The receiver chain starts with an analogue front end that can receive very small signals and digitise them using direct down conversion to in-phase (I) and quadrature (Q) baseband signals. down conversion is followed by analogue-to-digital conversion and a DDC that reduces the sampling rate and practises I and Q for transmission to a host computer using USB 3.0 for further processing. The transmitter chain starts with the host computer where I and Q are generated and transferred over the Ethernet cable to the USRP hardware. A DUC prepares the signals for the DAC after which I-Q mixing occurs to directly up convert the signals to produce an RF frequency signal, which

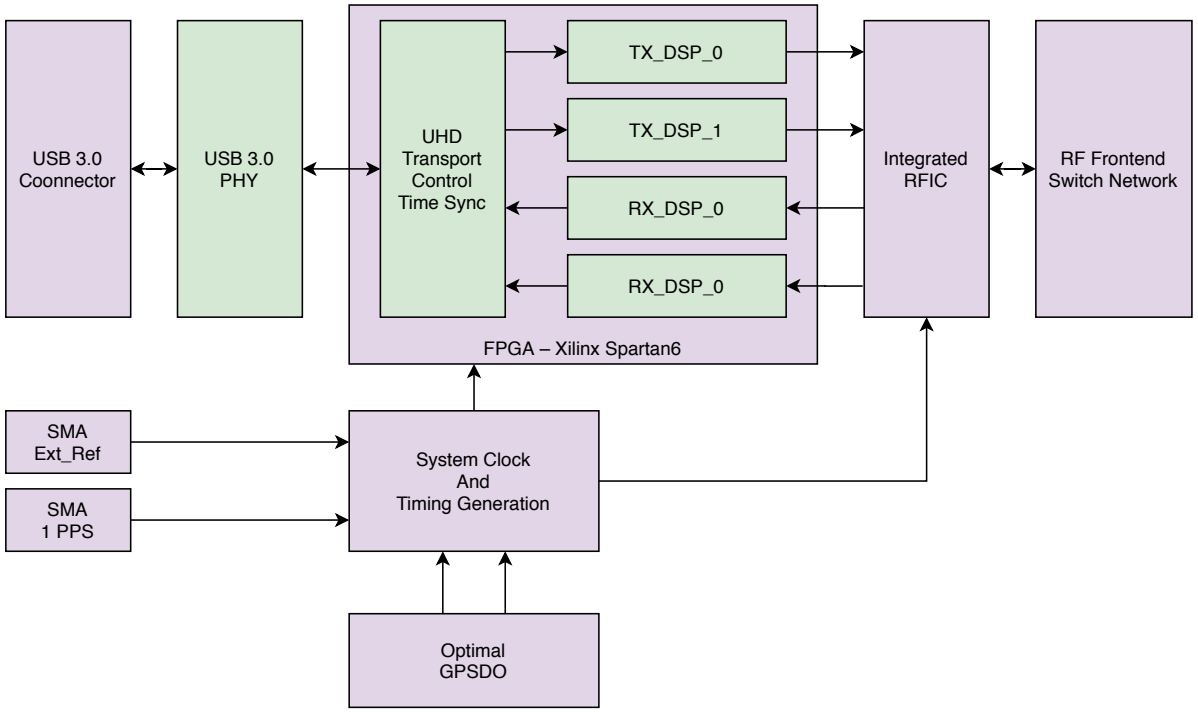

Figure 5.3: A diagram of internal components composing the SDR unit USRP B210 by Ettus Research.

is then amplified and transmitted—assuming no addition RF front end is connected the SDR.

For the BiSAD, however, an RF front end is added to up convert to and down convert from the X-band.
Table 5.2 provides the specifications of USRP B210 device according to the datasheet given in [5]. It is important for the radar system design to have the maximum available bandwidth of the SDR. The bandwidth of the USRP device varies at each point of the signal chain in Figure 5.4. Generally, the maximium available bandiwdth of the SDR is the minimum bandwidth of host, FPGA processing, and the analogue RF board. The analogue instantaneous bandwidth in 2x2 mode is up to 30.72 MHz. The FPGA processing bandwidth is the sample rate by ADCs and DACs. This is 61.44 MS/s quadrature sampling full duplex. Finally, the host bandwidth is the interface data rate between the USRP device and a host PC. USRP B210 has a USB 3.0 interface. The theoretical data rate of USB 3.0 is 5 Gbit/s. However, the real data rate can be lower than that. According to the datasheet, the 16-bit (I/Q) host interface data rate, is 61.44 Ms/s. This means 1.96 Gbit/s. If we take 8-bit samples for I and 8-bit samples for Q and consider two received signals then we get 61.44 MS/s in dual receiver mode. However, if we take 12 samples for I and Q, and two received signals, we get 40.96 MS/s. Considering all this, we can have a maximum bandwidth of 20 MHz for 12-bit and 30 MHz for 8-bit in dual receiver mode.
Another important parameter to consider is the on-off switching time of the RF switch in the SDR as we would like to switch the SDR on when we transmit the pulse and off during the silent interval. Unfortunately, this parameter is not specified in the datasheet.

Table 5.2: USRP B210 specifications.

USRP B210		
ADC rate	61.44	MS/s
ADC resolution	12	bits
DAC rate	61.44	MS/s
DAC resolution	12	bits
Interface	USB 3.0	-
Host sample rate (16-bit, I/Q)	61.44	MS/s

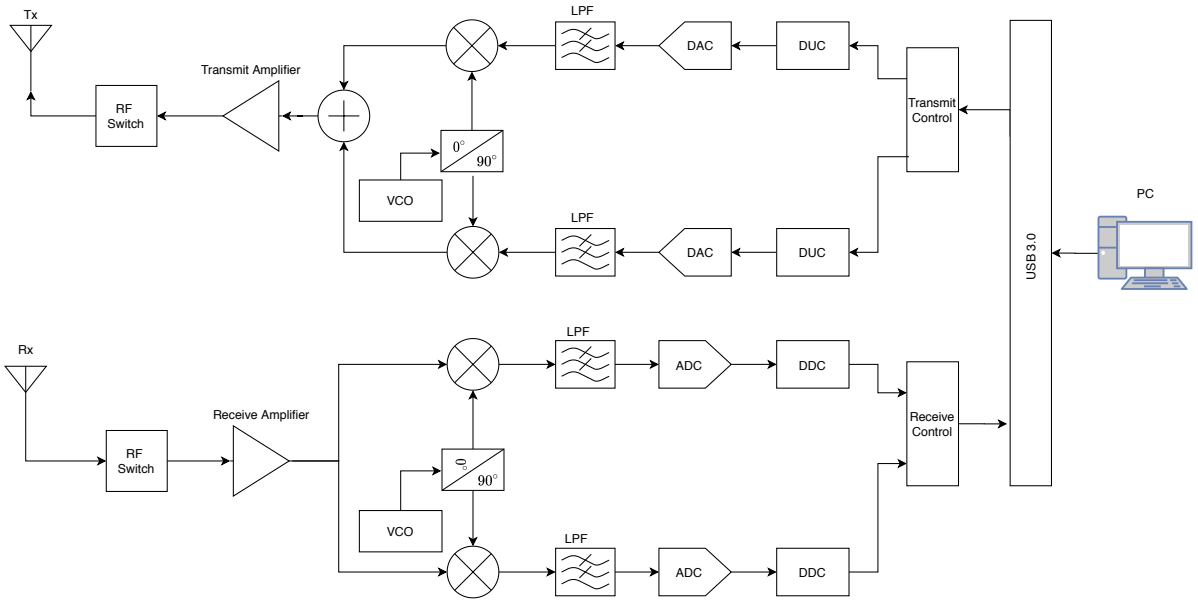

Figure 5.4: General hardware architecture of USRP SDR.

6

Results and System Evaluation

The waveform we are considering in this project is an LFM waveform due to its many advantages. As we have discussed Chapter 4, the bandwidth must be as high as possible. According to the specification of the chosen SDR, the bandwidth can be as high as 20 MHz. From the range requirements of the project, R_t can be up to 50 km and R_r is up to 5 km, then the repetition frequency according to Equation (4.1) is:

$$f_p \leq 5.45\,\text{kHz} \tag{6.1}$$

As stated in the radar equation (Equation (3.20)), longer pulse width τ increases transmit energy, hence increases the SNR. Our aim is to transmit the highest possible energy that the antenna is capable of. Nevertheless, increasing the pulse width forces us to decrease the pulse repetition frequency f_p. High pulse repetition frequency f_p is desired in order to keep the processing interval for the detection short, more detection decisions per unit time. Another approach is to consider coherent pulse integration, where train of pulses is transmitted with the maximum allowable f_p while the antenna beam is pointing at the target. Adding the multiple return pulses of the target, increases the SNR, motivated by the idea that the interference averages out. However, due to time limitations we considered target detection based on only one pulse. For this single pulse detection, we consider $\tau = 0.2\,\text{ms}$ and $f_p = 1\,\text{kHz}$.
If the antenna beam is pointing at both receiver and the target, we can write the ratio of the received echo power P_r to the power received form the direct line of sight P_{rd}. By comparing Equations (3.16) and (3.15) we can write:

$$\frac{P_r}{P_{rd}} = \frac{\sigma}{4\pi}\frac{L^2}{R_t^2 R_r^2} \tag{6.2}$$

From this equation we can calculate the worst-case scenario where L is minimised and $R_t R_r$ is maximised. If we consider $\beta = 0$, then $L_{min} = 2.5\,\text{km}$ and $(R_t R_r)_{max} = 37.5\,\text{km}^2$ (equivalent to $37.5 \times 10^6\,\text{m}^2$) and $\sigma = 1\,\text{m}^2$, this results in $P_r / P_{rd} = -94.5\,\text{dB}$. Considering this, we have chosen a Blackman-Harris window.
Table 6.1 summarises the waveform parameters combined with the parameters of transmitter and receiver chain. Based on these parameters, we evaluate the system performance in the following sections.

6.1. Range Resolution

The range resolution of the bi-static radar can be calculated using Equation (3.8) with a compressed pulse width of $\tau_c = 0.2\,\mu\text{s}$. Figure 6.1 shows the range resolution for $-140^\circ \leq \beta \leq +140^\circ$. Form the figure, we can conclude that the worst-case range resolution is $\Delta R_B = 88\,\text{m}$ at $\beta = \pm 140^\circ$ while the best resolution is $\Delta R_B = 30\text{m}$ at $\beta = 0^\circ$, which corresponds to a monostatic case. The MATLAB code to produce range resolution figure is given in Appendix A.5.

Table 6.1: System parameters.

Transmitter		
Peak power (P_t)	3.03	W
Antenna gain (G_t)	27	dB
Waveform		
Pulse duration (τ)	0.2	ms
Compressed pulse duration (τ_c)	0.2	us
Bandwidth (B)	20	MHz
Pulse repetition interval (PRI)	1	ms
Processing gain (G_p)	36	dB
Carrier frequency (f_c)	9.7	GHz
Receiver		
Antenna gain (G_r)	2	dB
Noise Figure (F)	3	dB
System Losses		
Losses (L_s)	3	dB

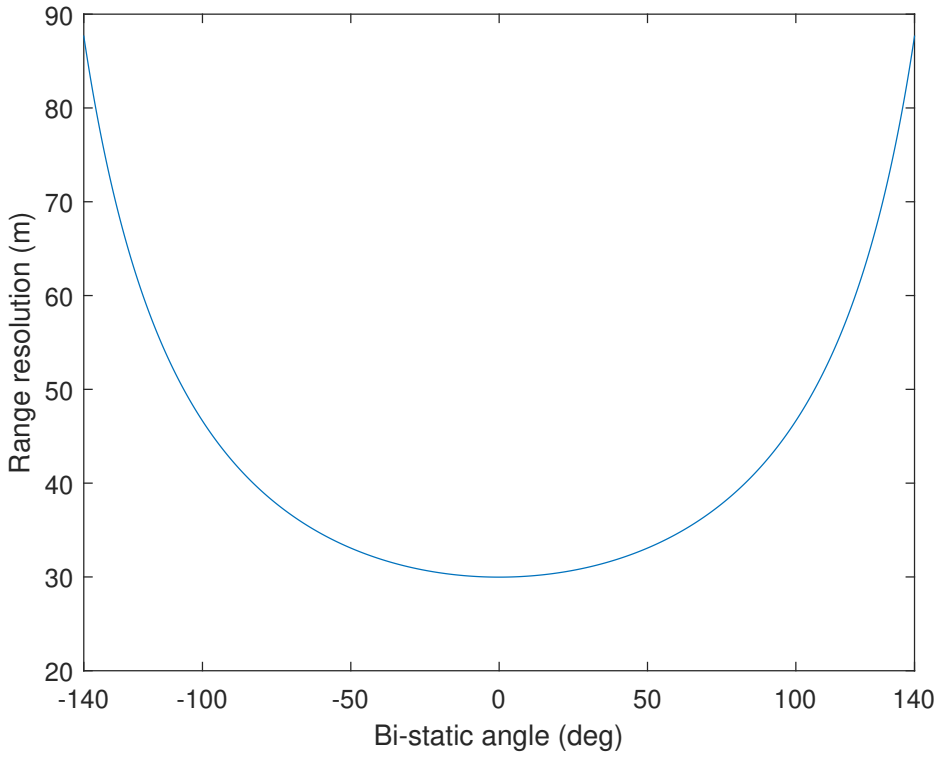

Figure 6.1: Bi-static range resolution for $-140° \leq \beta \leq +140°$

.

6.2. Blind Range

The blind zone of the radar describes regions in the bi-static plane where the target cannot be detected. Recall Equation (3.1):

$$R_t + R_r = c\Delta T + L \tag{6.3}$$

As discussed in Chapter 3, the solutions of $R_t + R_r$ are described by isorange contours. When ΔT (time difference between direct and reflected path peaks) is smaller than the compressed pulse width τ_c, the target is not detectable anymore and the resulted isoranges called the minimum isorange contours.

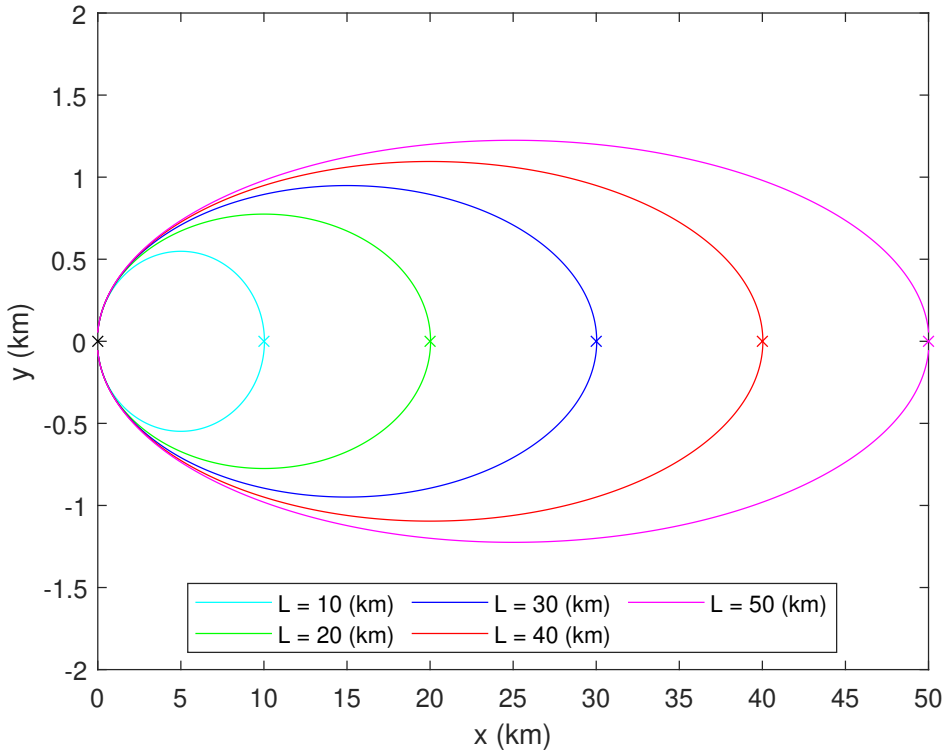

Figure 6.2: The blind range zones for different values of the baseline $L = [5, 10, 20, 30, 40, 50]$ km and $\tau_c = 0.2\mu$s.

In a monostatic radar, the blind zone region is a circle surrounding the transmitter/receiver. However, in a bi-static radar the circle becomes an ellipse that varies in shape according to the distance L. Figure 6.2 shows the blind zone regions (regions within ellipses) of the bi-static radar for different baselines and a compressed pulse width $\tau_c = 0.2\mu$s. As can be seen, the blind region gets bigger as the baseline distance increases. From the requirements of the project, $L_{max} = 50$ km and the target should be detectable around the receiver within 5 km distance. For better visualisation, we can plot a circle around the receiver which indicates the region in which the target should be detectable. This is shown in Figure 6.3a and 6.3b. The red circle in Figures 6.3a and 6.3b (a zoomed in version) highlights the 5 km range around the receiver in which targets should be detectable. All targets located inside the minimum isorange depicted by the blue ellipse in Figure 6.3b are undetectable by the bi-static radar. Moreover, the target is not detectable when it is located on the baseline. Using MATLAB, the blind range can be investigated based on transmitter and receiver locations in two dimensional plane. Using Cartesian coordinates, the transmitter and the receiver have the coordinates (x_t, y_t) and (x_r, y_r), respectively. We start by substituting ΔT with τ_c in Equation (6.3). The angle between the transmitter and receiver is computed using Equation (6.5). Equations (6.6) and (6.7) express the semi axes of the ellipse. The ellipse representing the isorange can be expressed in parametric form as stated in Equation (6.9), however, in order to draw the correct representation the ellipse should be rotated using the rotation matrix $\boldsymbol{R}$ and translating the centre of the ellipse to middle of the baseline using the vector $\boldsymbol{c}$. Equation (6.11) provides a complete representation of the minimum isorange.

$$R_t + R_r = c\tau_c + L \tag{6.4}$$

$$\alpha = \tan^{-1}\left(\frac{y_r - y_t}{x_r - x_t}\right) \tag{6.5}$$

$$a = (R_t + R_r)/2 \tag{6.6}$$

$$b = \sqrt{a^2 - \left(\frac{L}{2}\right)^2} \tag{6.7}$$

$$\boldsymbol{c} = \begin{bmatrix} x_0 \\ y_0 \end{bmatrix} = \begin{bmatrix} x_t + (x_r - x_t)/2 \\ y_t + (y_r - y_t)/2 \end{bmatrix} \tag{6.8}$$

$$\boldsymbol{A} = \begin{bmatrix} x \\ y \end{bmatrix} = \begin{bmatrix} a\cos\theta \\ b\sin\theta \end{bmatrix}, \quad -\pi \leq \theta \leq \pi \tag{6.9}$$

$$\boldsymbol{R} = \begin{bmatrix} \cos\alpha & -\sin\alpha \\ \sin\alpha & \cos\alpha \end{bmatrix} \tag{6.10}$$

$$\boldsymbol{A_c} = \boldsymbol{R}\boldsymbol{A} + \boldsymbol{c} \tag{6.11}$$

A MATLAB function that generates the blind zone plot based on transmitter and receiver locations is given in Appendix A.6.
The blind range is inherent to the bi-static radar. However, it can be improved by decreasing the compressed pulse width. In other words, increasing the sweep bandwidth B of the LFM waveforms reduces the size of the blind range zones.

In case of the proof of concept design, the maximum achievable separation distance of the transmitter and receiver is 2 km and maximum range of detectable target is 600 m as discussed in Section 6.4. Figure 6.4 illustrates the blind range of the bi-static radar in this configuration. As can be seen in the figure, targets with a bi-static angle $\beta = 180^\circ$ or $\beta \approx 150.6^\circ$ fall completely inside the blind range.

6.3. Range accuracy

The range accuracy of the radar is the certainty with which the distance to the target is known. We only consider the effect the Doppler shift on range measurement accuracy. As discussed in Chapter 4, the Doppler shift affects the range measurement in two ways. First the response of the matched filter will be delayed by $\left|f_d \frac{\tau}{B}\right|$. Second, the bandwidth of the waveform will be decreased as $B - |f_d|$. The Doppler shift is given in Equation (3.12). For simplicity, we consider stationary transmitter and receiver $|\mathbf{v_t}| = |\mathbf{v_r}| = 0\,\mathrm{m\,s^{-1}}$. Then, a maximum Doppler shift caused solely by the target motion can be written as:

$$\left|f_{dmax}\right| = \frac{2V_{max}}{\lambda} \tag{6.12}$$

Considering a maximum drone speed of $60\,\mathrm{m\,s^{-1}}$, results a maximum Doppler shift of $\left|f_{dmax}\right| \approx 4\,\mathrm{kHz}$. This yields a bandwidth of $B = 20\,000\,\mathrm{kHz} - 4\,\mathrm{kHz} = 19\,996\,\mathrm{kHz}$, and a maximum delay at the output of the matched filter as $\delta t = \left|f_d \frac{\tau}{B}\right| = 0.04\,\mu\mathrm{s}$ which results in an error in the range measurement. We define a relative error in the range measurements as:

$$error = \frac{R_{rA} - R_{rE}}{R_{rE}} \tag{6.13}$$

Where Rr_A is approximated range value (with error) and Rr_E is the exact range. Recall, that the exact range can be calculated using Equations (3.1), (3.5) and (3.6). The approximated range can be calculated by substituting ΔT with $\Delta T + \delta t$ in those equations where ΔT is the time difference between echo and direct peaks and δt is the extra delay due to Doppler shift.

Figure 6.5 shows the relative error as a function of the exact range. The error is plotted for different values of ΔT where 0.2 µs is the minimum observable delay. As we can see, the error is has a maximum value of 12% with a maximum Doppler shift. However, for longer delay ΔT the error is smaller and as the range R_r increases, the error decreases significantly.

6.4. SNR Evaluation Using Ovals of Cassini

To evaluate the performance of radar system, the SNR is investigated for the ranges specified in the requirements (Chapter 2) and the system parameters specified in Table 6.1. The requirements state that the radar system should be able to detect targets that are as far as 50 km from the transmitter and as far as 5 km from the receiver. Nonetheless, this range requirement does not apply to the proof of concept design proposed in this thesis. The ovals of Cassini represent positions in the 2D Cartesian space that have the same SNR value for a constant range product $R_t R_r$. Depending on the SNR value and assuming a target with Swerling-1 model—as expressed in Equation (3.23)—the probability of detection P_d and the probability of false alarm P_{fa} are

traded off. This trade-off is shown in the receiver operating characteristic curve Figure 6.6—ROC curve for short. The sweet spot in Figure 6.6 is located in the top left corner, where the probability of detection is high and the probability of false alarm is low. Moreover, Figure 6.6 shows that the higher the SNR is, the better the trade-off will be, i.e. P_d is as high as possible and P_{fa} is as low as possible. Considering a probability of detection of 90% a desirable detection rate, then for single pulse detection and Swerling-1 targets, an SNR of 10 dB yields a probability of false alarm around 31%.

Analysing the SNR value using the ovals of Cassini, Figure 6.7 shows that the targets at ranges $R_t = 50\,\text{km}$ from the transmitter and $R_r = 5\,\text{km}$ from the receiver have extremely weak echoes. The low SNR renders these targets invisible since $P_d \approx P_{fa}$. Considering a minimum SNR of 10 dB, then the maximum range product $R_t R_r = 1.2\,\text{km}^2$. For example, a distance of $R_t = 2\,\text{km}$ results in a range of detection up to $R_r = 600\,\text{m}$ from the receiver. Figures 6.8 and 6.9 show Cassini ovals for different baseline distances, 2 km and 3 km, respectively.

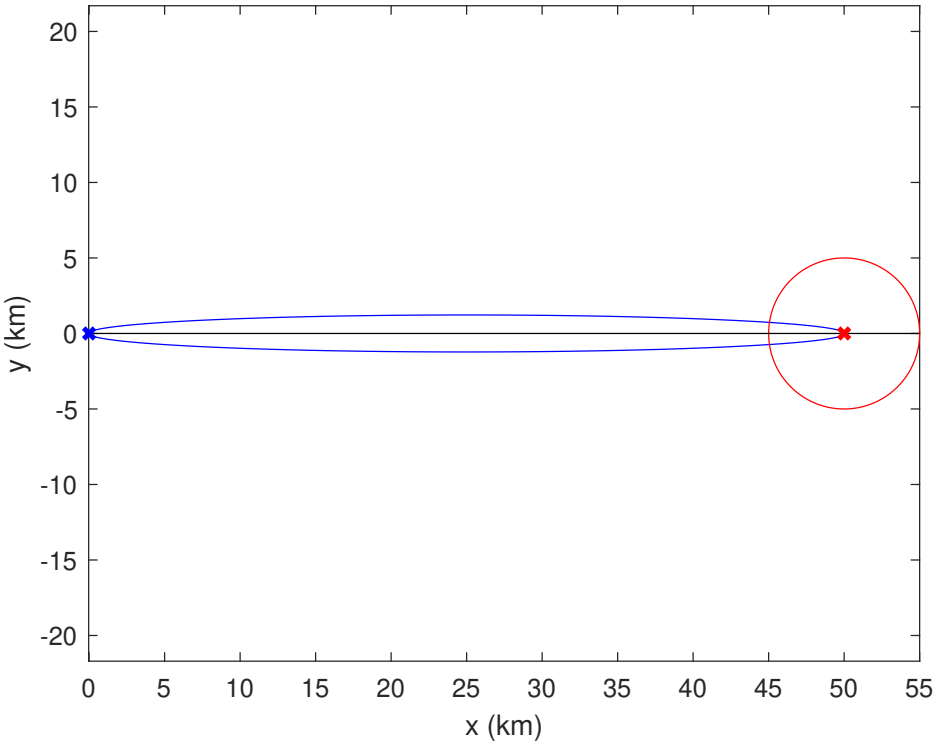

(a)

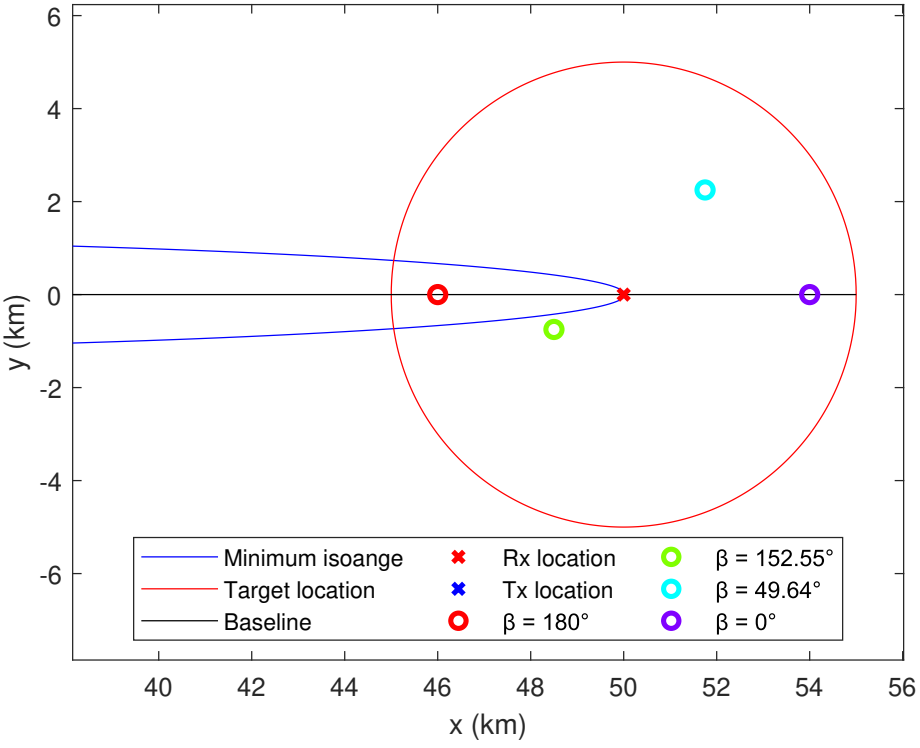

(b)

Figure 6.3: Blind range analysis of configuration with a base line $L = 50$ km and β is the bi-static angle in degrees. 6.3a shows the shape of the isorange in blue, 6.3b is zoomed in and shows some targets.

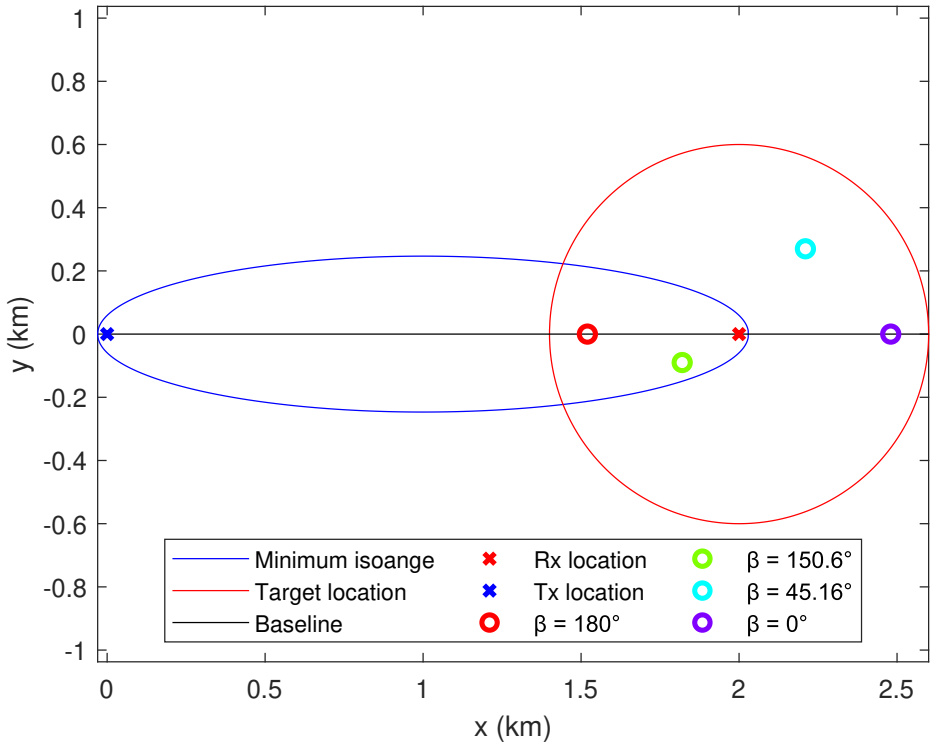

Figure 6.4: Blind range analysis of configuration with a base line $L = 2$ km and β is the bi-static angle in degrees.

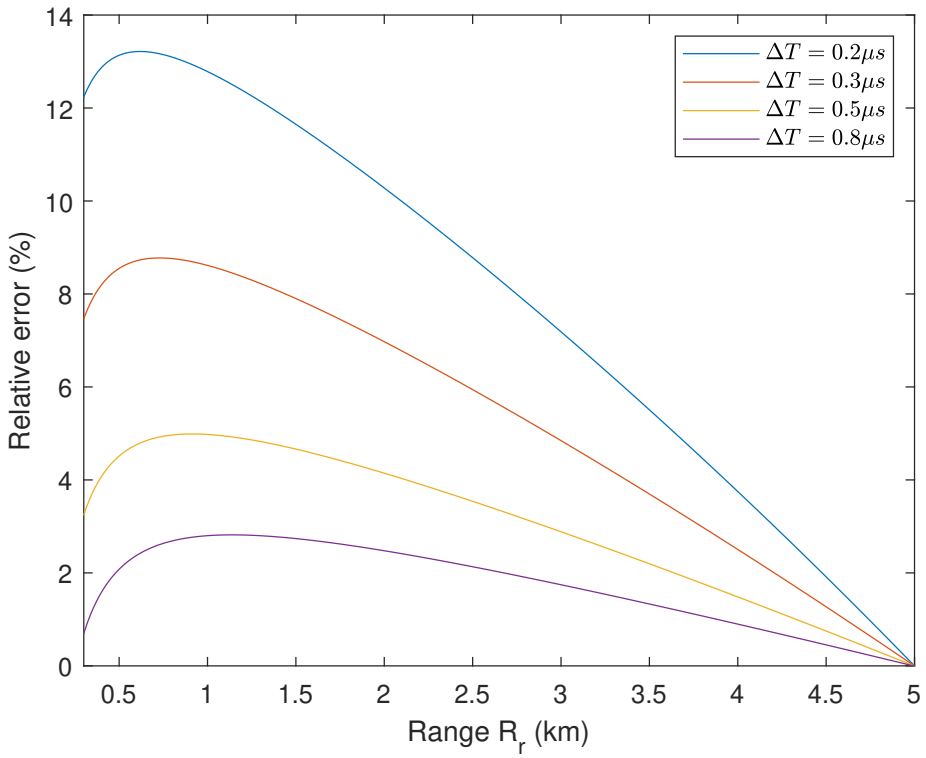

Figure 6.5: Relative error in range measurements for different ΔT and a maximum Doppler shift $f_d = 4$ kHz.

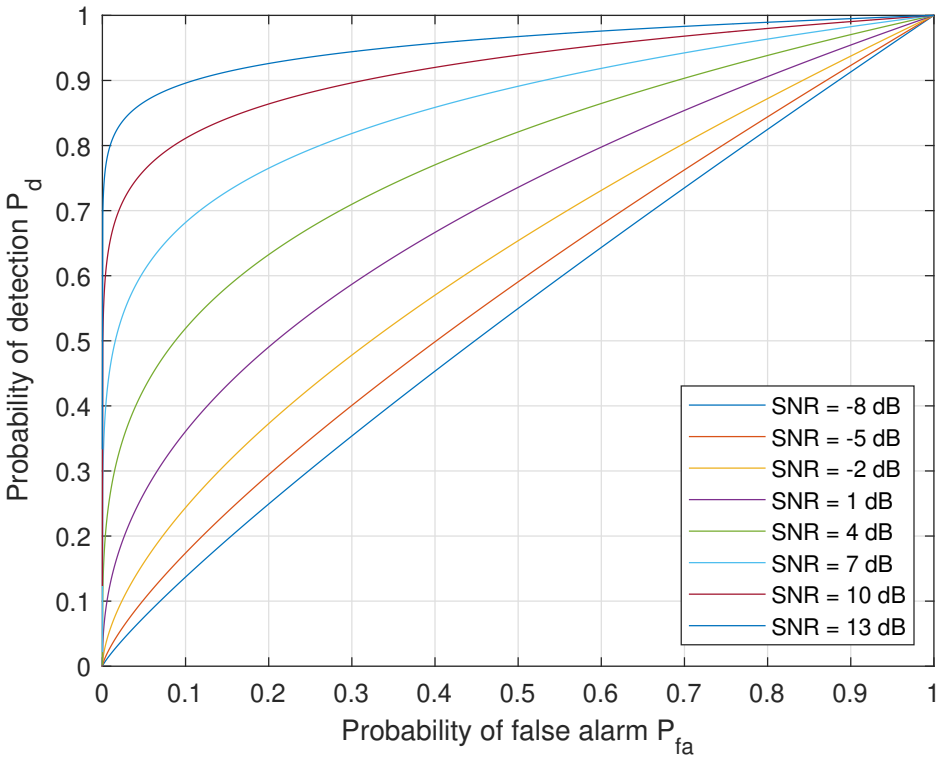

Figure 6.6: The ROC curves for single pulse detection and Swerling-1.

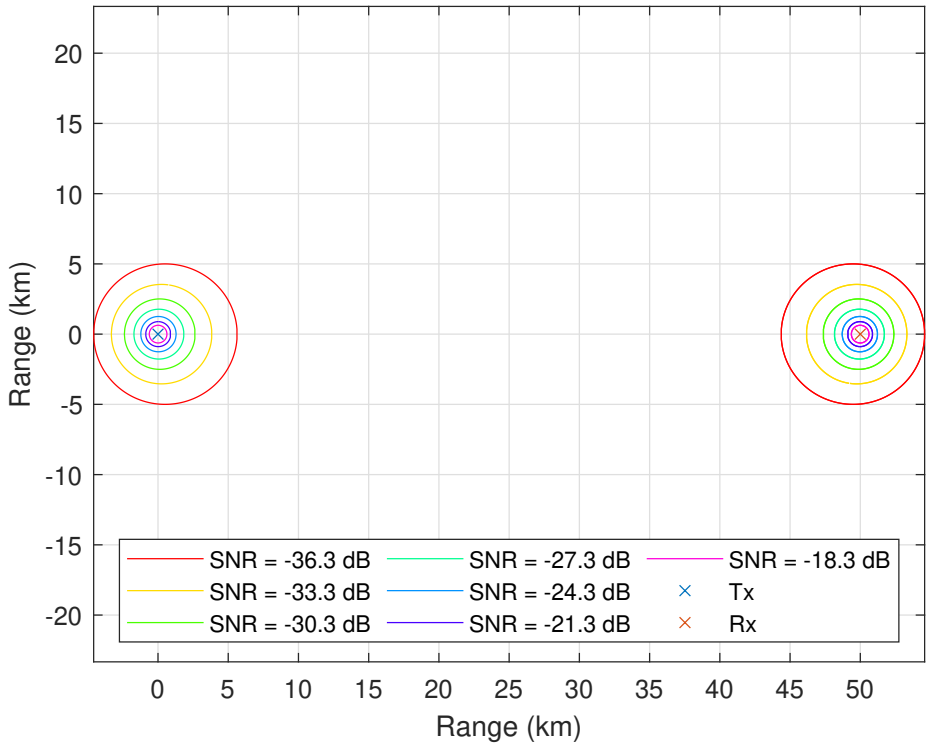

Figure 6.7: Evaluation of target detectability in terms SNR for $L = 50$ km.

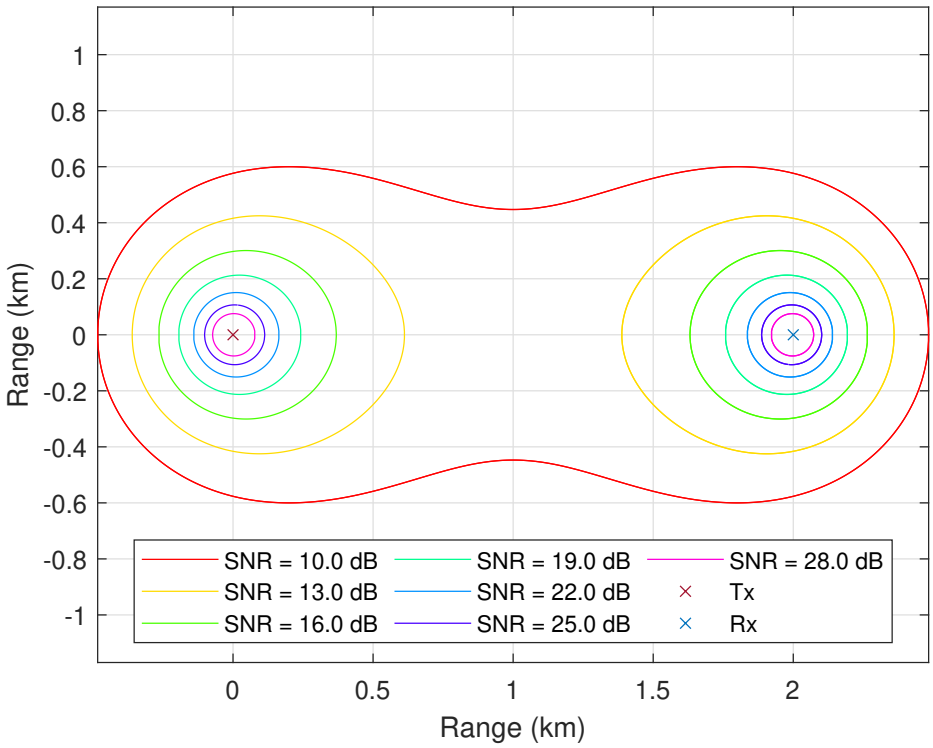

Figure 6.8: Evaluation of target detectability in terms SNR for $L = 2\,\text{km}$.

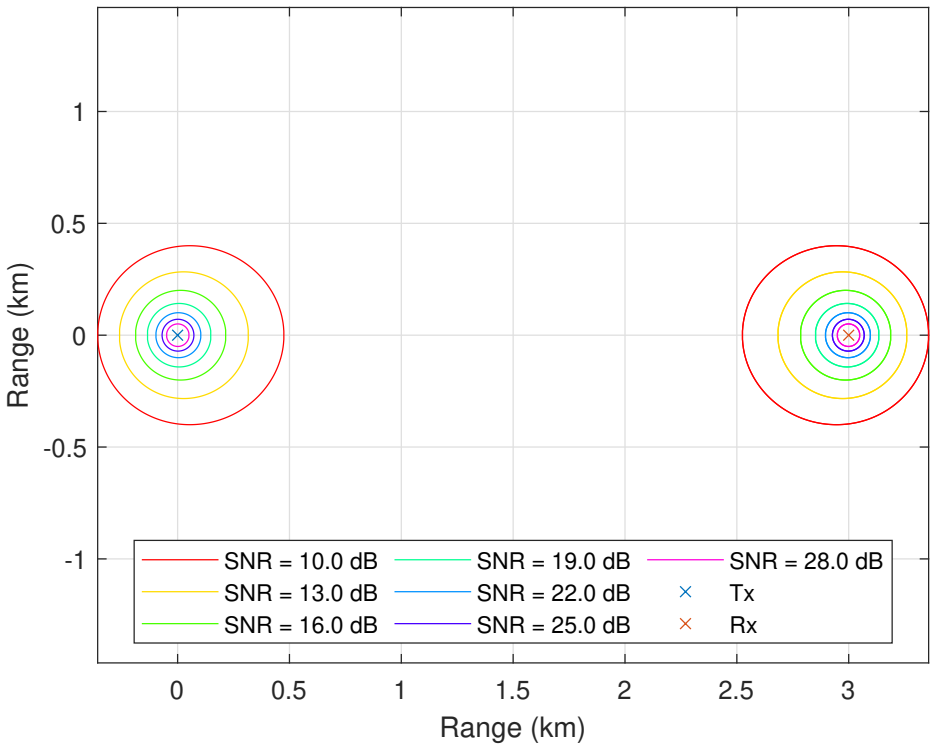

Figure 6.9: Evaluation of target detectability in terms SNR for targets for a separation distance of $L = 3\,\text{km}$ yielding a detection range around the receiver of $R_{r,\max} = 400\,\text{m}$.

7

GNU Radio Companion

GNU Radio Companion is a software that is used to implement signal processing for software radio applications[12, 15, 20]. GNU Radio can be used to program SDRs or it can be used without external RF hardware for simulation purposes. The selected SDR, the USRP B210, can be programmed with GNU Radio to generate and transmit the radar waveform. In addition, using GNU Radio we can program the SDR for signal reception at the receiver site such that signal processing for target detection is implemented.
First, GNU Radio implementations of the transmitter and receiver chains are discussed. And finally, a GNU Radio simulation of the entire system is provided.

7.1. Transmitter SDR

As described in Chapter 5, the SDR is responsible for generating the LFM waveform with a carrier frequency of 3.875 GHz and a local oscillator of 5.825 GHz for the up-converter in the transmitter chain. A GNU Radio schematic the transmitter SDR is shown in 7.1.

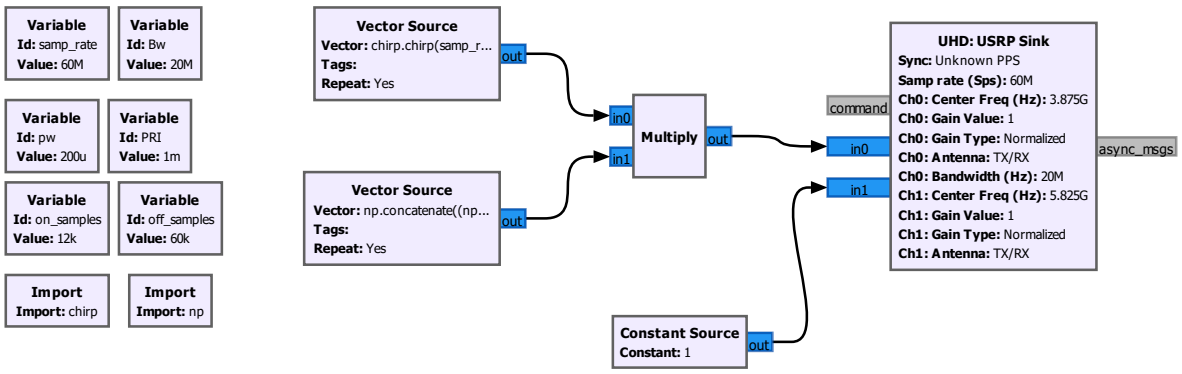

Figure 7.1: GNU Radio schematic for the transmitter SDR.

The variables shown at the left side of the schematic are used for the signal generation based on the LFM parameters sample rate (`samp_rate`), bandwidth (`Bw`), pulse width (`pw`) and pulse repetition interval (`PRI`). The variables `on_samples` and `off_samples` are used to calculate on-time and off-time of the waveform in sample unit. To generate the LFM waveform a Python function `chirp.py` is utilised, the code can be found in Appendix A.7. The function is imported using the import block `Import chirp`.
The vector source connected to the `in0` of the multiply block, generates the LFM waveform by calling the python function `chirp.py`. The block calls the function once and then the waveform is repeated. However, waveform is multiplied with a rectangle window for the specified PRI. The second vector source generates this window using the Python module Numpy (`np`). After multiplication the signal is connected to `USRP Sink` which is a transmitter block dedicated for USRP devices.
This approach of transmitting the LFM waveform may be problematic as we are multiplying the waveform

with a rectangle window. Therefore, zeros will be relayed to the transmitter block and hence noise will be generated, amplified and transmitted. A better approach is to switch the SDR off and on depending on the desired PRI. However, the datasheet of the SDR does not provide on-off switching times of the RF switch and hence measurements are required.
Finally, the second input of the `USRP Sink` block is connected to a `Constant Source`. This will generate the local oscillator needed as the centre frequency of this channel is 5.825 GHz.

7.2. Receiver SDR

A GNU Radio schematic the receiver SDR is shown in 7.2. `USRP Source` block is the receiver block of the USRB device. The block provides two channels for the two receiver antennas. The received signals are relayed to the `FFT Filter` block. This block applies matched filtering and Blackman-Harris windowing to the signals. This is done by using the Python function `mhr.py` provided in Appendix A.7. The function provides the needed taps for the FFT filter. The taps are stored in variable `MF_RS` which generates the taps based on the waveform parameters. Finally, the output of the FFT filter is converted to magnitude. and plotted in time domain using `Time Sink` block.

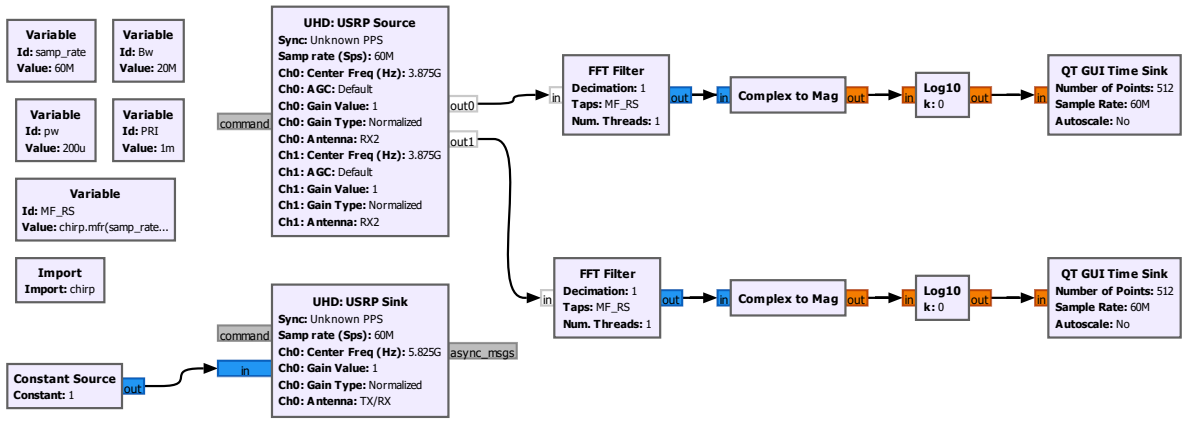

Figure 7.2: GNU Radio schematic for the receiver SDR.

Similar to the transmitter SDR, the `USRP Sink` block generates the local oscillator needed for analogue down-conversion of the RF signals during reception.

7.3. Radar Simulation

The radar system is simulated in GNU Radio without any of the SDR devices. A schematic of the simulation is shown in Figure 7.3. The system parameters used in the simulation are given in Table 6.1. In this simulation, the transmitter antenna beam is assumed to be pointing at both the receiver and target. First, the LFM waveform is generated. This is shown in the LFM Waveform rectangle. Then, the waveform is relayed to the transmitter chain where the signal is amplified. This is shown in Transmitter Gain rectangle where the maximum antenna gain is $G_t = 27\,\text{dB}$. The wave is guided through two propagation paths. The direct path and the target path. In both paths the signal is attenuated and delayed according to the locations of transmitter, receiver and target. The locations have been implemented in variables that can be adjusted in run-time. At the receiver side the signals are added and then amplified by the receiver antenna gain. This is shown in the Receiver Gain rectangle. The received signal is then added to a white Gaussian noise corresponding to the noise power of the system. Finally, matched filter and windowing are applied in the FFT filter block. The output is converted to magnitude and then plotted using `Time Sink` block.

Figures 7.4 and 7.5 show some examples of the output. The figures illustrate two peaks, a large one and small one. The first one corresponds to the direct path. After some delay, the peak corresponds to the target is observed. The time difference between the peaks can be calculated and estimate the range accordingly.

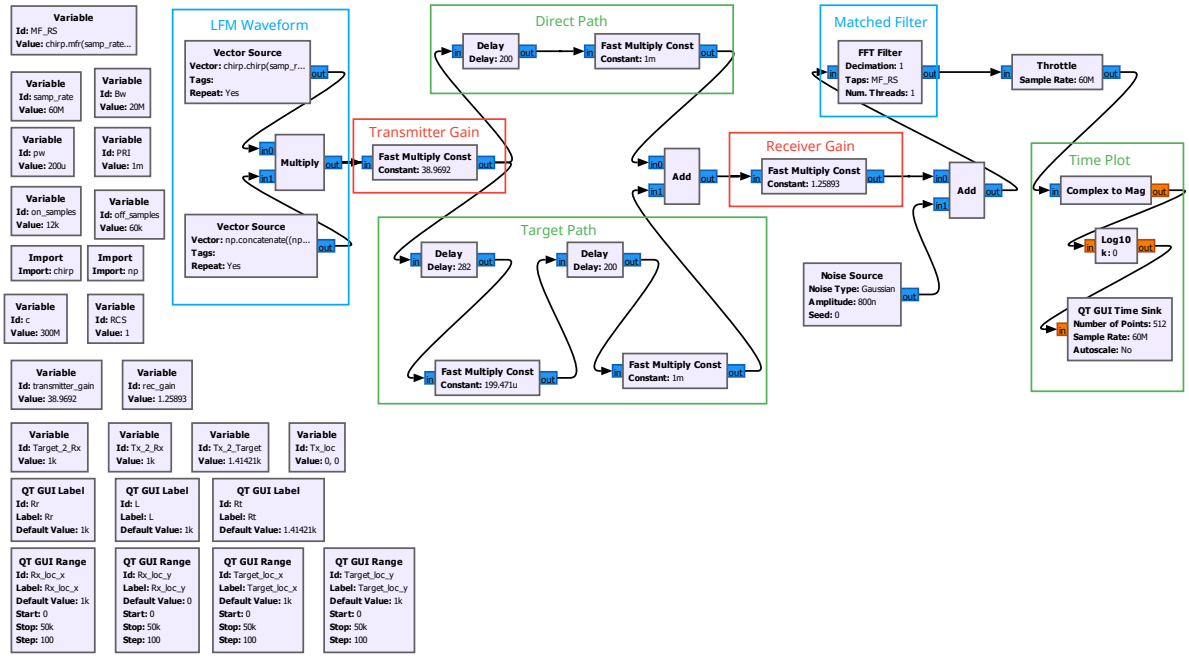

Figure 7.3: GNU Radio schematic for radar Simulation.

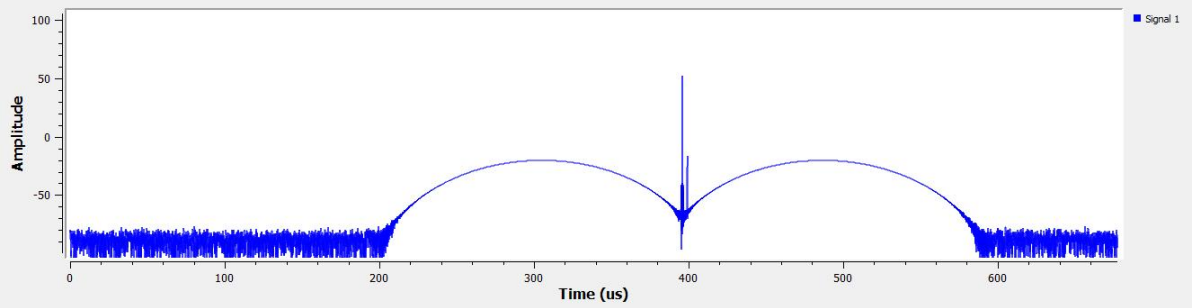

Figure 7.4: Simulation results for $L = 1\,\text{km}$, $R_t = 1.5\,\text{km}$ and $R_r = 500\,\text{m}$.

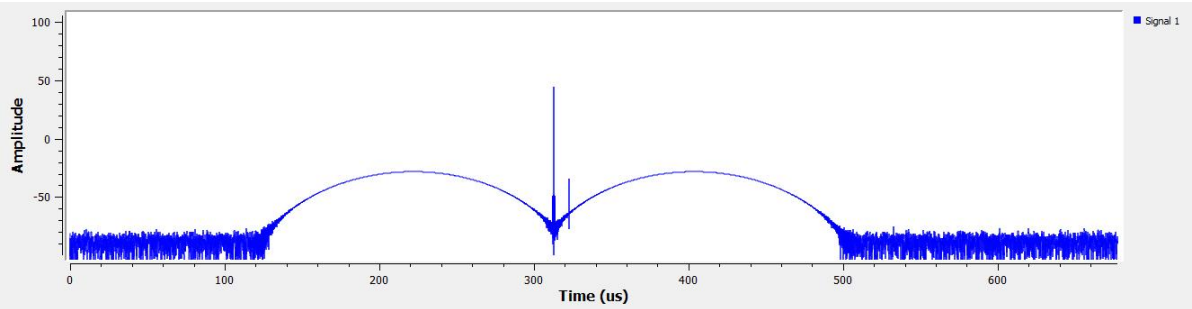

Figure 7.5: Simulation results for $L = 2.5\,\text{km}$, $R_t = 4\,\text{km}$ and $R_r = 1.5\,\text{km}$.

8

Conclusion and Future Work

The project's goal is to design a proof of concept bi-static radar system utilising solely commercially available off the shelf components. The design is comprised of a transmitter chain and a receiver chain, both based on SDR. Furthermore, a radar waveform design is proposed. Eventually, the main requirement for the actual bi-static radar system is capability of detecting targets as far as 50 km from the transmitter and as far as 5 km from the receiver. To satisfy this requirement, custom designed equipment is rather required instead of off the shelf components. Considering a peak power of $P_t = 3.02\,\text{W}$ transmitted by transmitter antenna whose gain is 27 dB and an LFM waveform with a pulse width $\tau = 0.2\,\text{ms}$ and a sweep bandwidth $B = 20\,\text{MHz}$, detection of targets is possible up to 2 km from the transmitter and up to 600 m from the receiver. This thesis evaluates single pulse detection and assumes Swerling-1 model. Evaluating the SNR values, targets located 2 km from the transmitter and 600 m can be detected with 90% probability of detection and 31% probability of false alarm. For targets any farther, the SNR gets degraded by a factor $R_t^2 R_r^2$. Placing a target for example at distance of 50 km away from the transmitter and 5 km away from the receiver while keeping the design unchanged, brings down the SNR to −36.3 dB, i.e. the signal at this point is simply drowned in noise hence rendering the target invisible for the radar system.

Target detection based on only one pulse is seldom used in radar systems. Usually, coherent pulse integration is employed to detect a target based on a train of pulses. Using coherent pulse integration increases the SNR by introducing a gain equals to the number of pulses coherently integrated. Therefore, considering pulse integration increases the maximum detectable range without increasing transmitting power. Detailed information regarding pulse integration is given in [14].
Furthermore, bi-static radar range resolution and blind region can be improved by increasing the waveform bandwidth. However, SDRs with bandwidths higher than 20 MHz, are expensive. Another option is to use NLFM (nonlinear frequency modulation) waveform. The disadvantage of LFM is that it has a high peak side lobe ratio and this requires a window to reduce it to a desired level. We have proposed Blackman-Harris window as it offers the best reduction of sidelobes such that targets pulses are not suppressed due to direct path pulses. However, Blackman-Harris window decreases the resolution by a factor of 4. NLFM waveform offers better peak sidelobe ratio and hence using this waveform may lead to the use of other windows that offer smaller reduction of the mainlobe width and hence a better resolution.
Finally, the GNU radio simulation of the radar system can be improved by including the transmitter antenna pattern and rotation. This gives a better representation of the system in the simulations.

Appendices

A

Supporting MATLAB code

A.1. Radar Equation

```
%% radarequation loads the system parameters of the radar design.
disp('Preparing system parameters and calculating the radar equation...')
%% Physical constants
c = physconst('Lightspeed');     % Speed of light (m/s)
k = physconst('Boltzmann');      % Boltzmann's constant
T0 = 290;                        % Temperature (K)
sigma = 1;                       % Radar cross section (m^2)

%% Waveform Parameters
B = 20e6;                        % Bandwidth (Hz)
tau = 200e-6;                    % Pulse duration (s)
Gp = B*tau;                      % Processing gain
f_c = 9.7e9;                     % Centre frequency (Hz)
lambda = c/f_c;                  % Wavelength (m)

%% Transmitter chain
Pt = 3.03;                       % Peak transmit power (W)
Gt = 27; Gt = db2pow(Gt);        % Antenna gain (dB)
Lt = 0; Lt = db2pow(Lt);         % Transmitter insertion losses (dB)

%% Receiver chain
Gr = 2; Gr = db2pow(Gr);         % Receiver gain (dB)
Lr = 3; Lr = db2pow(Lr);         % Receiver losses in system (dB)
NF = 3; F = db2pow(NF);          % Noise figure at receiver (dB)
N = k*T0*F*B;                    % Noise power

%% Radar equation
K = (Pt*Gt*Gr*Gp*((lambda)^2))/(((4*pi)^3)*Lr*Lt*N);
```

A.2. Radar Waveform

```
function [x,t]  = radarlfm(Fs,B,tau,Fc)
%RADARLFM generates an LFM waveform.
%
%   [x,t] = radarLFM(Fs, B, tau) generates a baseband LFM signal.
%   [x,t] = radarLFM(Fs, B, tau, Fc) in case of non-zero carrier frequency
    .
%
%   - Fs  = Sample frequency (Hz)
%   - B   = Bandwidth (Hz)
%   - tau = Pulse width (s)
%   - Fc  = Carrier frequency (Hz)
    arguments
        Fs  (1,1) {mustBeNumeric,mustBeReal}
        B   (1,1) {mustBeNumeric,mustBeReal}
        tau (1,1) {mustBeNumeric,mustBeReal}
        Fc  (1,1) {mustBeNumeric,mustBeReal} = 0
    end
    n = Fs*tau;                % Number of data points
    t = linspace(0,tau,n);     % Time base (s)
    wc = 2*pi*Fc;
    % Complex envelope
    x =  exp(1j* ((wc .* t) + (pi * (B/tau)* t.^2)));
end
```

A.3. Matched Filter

```
function h = matchedfilter(x,x_ref,w)
%MATCHEDFILTER computes the matched filter response.
%
%   h = matchedfilter(x,x_ref,w)
%   - x     = input signal
%   - x_ref = reference signal
%   - w     = specifies the window function
    arguments
        x       (:,:) {mustBeNumeric}
        x_ref   (:,:) {mustBeNumeric}
        w       (1,1) {mustBeNumeric} = 1
    end
    x = x(:);
    x_ref = x_ref(:);
    if w==2
        h_t = x_ref.*blackmanharris(length(x_ref));
    elseif w==3
        h_t = x_ref.*hamming(length(x_ref));
    else
        h_t = x_ref;
    end
    h = conv(x,conj(flipud(h_t)),'same');
    h = h';
end
```

A.4. LFM Waveform and Matched Filter Response

```
%% Generate LFM waveform
radarequation
Fs = 20*B;              % Sampling frequency (Hz)
n = Fs*tau;             % Number of data points
t = linspace(0,tau,n);  % Time vector (s)
u = radarlfm(Fs,B,tau); % Complex envelope

%% Matched filter response
y = matchedfilter(u,u,2); % Matched filter output with Blackman-Harris.
y = abs(y);               % Convert to absolute
y= y./(max(y));           % Normalize
y = 20*log10(y);
figure
plot(t*1e6, y)
xlabel('Time (us)');
ylabel('Amplitude (dB)');
title('Matched Filter Response for LFM Waveform')
```

A.5. Range Resolution

```
function [beta,res] = bistaticrangeresolution(B)
%BISTATICRANGERESOLUTION calculates the bistatic range resolution
%   corresponding to the sweep bandwidth B for -170 < beta < 170 deg,
%   given an LFM waveform is used in combination with
%   a Blackman-Harris window.
%
%   [beta,res] = bistaticrangeresolution(B)
%   - B     = sweep bandwith (Hz)
%   - beta  = bistatic angle (deg)
%   - res   = range resolution (m)
    c = physconst('Lightspeed');            % Speed of light (m/s)
    tau = 4/B;  % Compressed pulse duration with Blackman-Harris

    beta = linspace(-170,170,1e6);
    res = (c*tau)./(2*cos(deg2rad(beta)/2)); % Range resolution

    % Plot range resolution as function of bi-static angle
    figure
    plot(beta,res)
    xlabel('Bi-static angle (deg)');
    ylabel('Range resolution (m)');
    xlim([-140, 140])
end
```

A.6. Blind Range

```
function [xr,yr] = minisorange(tx,rx,plt,radius,targets,n)
%MINISORANGE computes and plots the blind range corresponding to the
%position of transmitter and receiver.
% - tx      = position of transmitter
% - rx      = position of receiver
% - plt     = swith on/off the plot
% - radius  = radius of circle around raceiver
% - targets = position of targets in a matrix
% - n       = number of data points
%
% - Example 1: calculate the coordinates of points on the isorange.
%   [xr,yr] = minisorange(tx,rx)
%
% - Example 2: calculate the coordinates of points on the isorange and
   plot
%   the isorange.
%   [xr,yr] = minisorange(tx,rx,1)
%
% - Example 3: calculate the coordinates of points on the isorange, plot
%   the isorange and the specified targets.
%   [xr,yr] = minisorange(tx,rx,1,3e3,targets)
%
% - Example 4: calculate the coordinates of points on the isorange, plot
%   the isorange and the specified targets.
%   [xr,yr] = minisorange(tx,rx,1,3e3,targets)
%
% - Example 4: calculate the coordinates of points on the isorange, plot
%   the isorange, the specified targets and specify the number of data
   points.
%   [xr,yr] = minisorange(tx,rx,1,50e3,targets,n)
    arguments
        tx      (:,:) {mustBeNumeric,mustBeReal}
        rx      (:,:) {mustBeNumeric,mustBeReal}
        plt     (1,1) {mustBeNumeric,mustBeReal} = 0
        radius  (1,1) {mustBeNumeric,mustBeReal} = 5e3
        targets (:,:) {mustBeNumeric,mustBeReal} = []
        n       (1,1) {mustBeNumeric,mustBeReal} = 1e6
    end
    radarequation
    tau = 4/B;
    L = norm(tx - rx);          % Distance between transmitter and
       receiver
    Rt_Rr = c*tau + L;          % Distance traveled by echo

    a = Rt_Rr/2;                % Horizontal major semi-axis of the
       ellipse
    b = sqrt(a^2 - (L^2)/4);    % Vertical minor semi-axis of the ellipse

    x0 = ((rx(1) - tx(1))/2) + tx(1); % x0 ellipse centre coordinates
    y0 = ((rx(2) - tx(2))/2) + tx(2); % y0 ellipse centre coordinates
    t = linspace(-pi,pi,n);     % Angle
    x = a*cos(t);               % x-component
    y = b*sin(t);               % y-component
```

```
    alpha = atan((rx(2) - tx(2))/(rx(1) - tx(1)));
    R  = [cos(alpha) -sin(alpha); sin(alpha) cos(alpha)]; % Rotation
       matrix
    r_coor = R*[x; y];          % Points on the ellips
    xr = r_coor(1,:)' + x0;     % Translation along the x-axis
    yr = r_coor(2,:)' + y0;     % Translation along the y-axis
    if plt
        colors = hsv(length(targets));
        figure
        plot(xr*1e-3,yr*1e-3,'b','DisplayName','Minimum isoange')
        lgd = legend;
        % axis equal
        hold on

        % Target locations
        theta  = linspace(0,360,n); theta  = deg2rad(theta);
        xloc   = radius*cos(theta) + rx(1);
        yloc   = radius*sin(theta) + rx(2);

        plot(xloc/1e3,yloc/1e3,'r','DisplayName','Target location')

        % Base line
        m = (rx(2) - tx(2))/(rx(1) - tx(1));
        b = tx(2) - (m * tx(1));
        base_x = linspace(tx(1),rx(1) + sign(rx(1))*radius*cos(alpha),n);
        base_y = m*base_x + b;
        plot(base_x/1e3,base_y/1e3,'k','DisplayName','Baseline')

        scatter(rx(1)/1e3,rx(2)/1e3,'x','r',...
            'LineWidth',2,...
            'DisplayName','Rx location');       % Receiver location
        scatter(tx(1)/1e3,tx(2)/1e3,'x','b',...
            'LineWidth',2,...
            'DisplayName','Tx location');       % Transmitter location

        [i_max,~] = size(targets);
        if i_max > 0
           colors = hsv(i_max);
           for i = 1:i_max
                target = targets(i,:);
                beta = bistaticangle(tx,rx,target);
                scatter(target(1)/1e3,target(2)/1e3,40,'o',...
                    'MarkerEdgeColor',colors(i,:),...
                    'LineWidth',2,...
                    'DisplayName', ['beta = ',num2str(beta),' (deg)']);
            end
        end
        xlabel('x (km)')
        ylabel('y (km)')
        title('Detection and blind zone')
        lgd = legend('location','south');
        lgd.NumColumns = 3;
        hold off
        axis equal
    end
end
```

```
function beta = bistaticangle(tx,rx,target)
%BISTATICANGLE
%   calculates the bistatic angle given the coordinates of the transmitter
%   receiver, and target.
%   beta = bistaticangele(tx,rx,target)
    u = target - tx; u = [u 0];
    v = target - rx; v = [v 0];
    beta = atan2(norm(cross(u,v)),dot(u,v));
    beta = round(rad2deg(beta),2);
end
```

A.7. Python LFM Waveform and Matched Filtering for GNU Radio

```
import numpy as np
import scipy.signal.windows as win  # import window functions


# Function to generate LFM waveform
# Inputs: fs (sampling rate) pulse duration and bandwidth
# Outputs: Complex envelope of LFM
def chirp(fs, pulse_duration, bandwidth):
    n = int(fs * pulse_duration)
    t = np.linspace(0, pulse_duration, n)
    k = bandwidth / pulse_duration
    t_2 = np.square(t)
    u = np.exp(1j * np.pi * k * t_2)
    return u


# Function to generate matched filter taps for FFT filter
#  with Blackman-Harris windowing
# Inputs: fs (sampling rate) pulse duration and bandwidth
# Outputs: FFT taps
def mfr(fs, pulse_duration, bandwidth):
    u = chirp(fs, pulse_duration, bandwidth)
    window = win.blackmanharris(len(u))
    u = u * window
    s = np.conj(u)
    s = np.flip(s)
    return s
```

Bibliography

[1] Evan Ackerman and Michael Koziol. The blood is here: Zipline's medical delivery drones are changing the game in Rwanda. *IEEE Spectrum*, 56(5):24–31, may 2019. doi: 10.1109/mspec.2019.8701196.

[2] Ed Alexander and D Poularikas. The handbook of formulas and tables for signal processing. *Boca Raton, FL, USA: CRC Press*, 73:79, 1998.

[3] James WA Brown. *FM Airborne Passive Radar*. PhD thesis, UCL (University College London), 2013.

[4] Leon W. Couch. *Digital and Analog Communication Aystems*. Pearson/Prentice Hall, 8 edition, 2007.

[5] *USRP B200/210 Bus Series*. Ettus Research, 2019. URL `https://www.ettus.com/wp-content/uploads/2019/01/b200-b210_spec_sheet.pdf`.

[6] Hugh Griffiths and Nicholas Willis. Klein heidelberg—the first modern bistatic radar system. *IEEE Transactions on Aerospace and Electronic Systems*, 46(4):1571–1588, oct 2010. doi: 10.1109/taes.2010.5595580.

[7] Samer Baher Safa Hanbali. A review of radar signals in terms of doppler tolerance, time-sidelobe level, and immunity against jamming. *International Journal of Microwave and Wireless Technologies*, 10(10): 1134–1142, aug 2018. doi: 10.1017/s1759078718001174.

[8] M. C. Jackson. The geometry of bistatic radar systems. *IEE Proceedings F - Communications, Radar and Signal Processing*, 133(7):604–612, 1986.

[9] Young-Kil Kwag, Jung-Soo Jung, In-Sang Woo, and Myeong-Seok Park. Multi-band multi-mode SDR radar platform. In *2015 IEEE 5th Asia-Pacific Conference on Synthetic Aperture Radar (APSAR)*. IEEE, sep 2015. doi: 10.1109/apsar.2015.7306151.

[10] Young-Kil Kwag, In-Sang Woo, Ho-Young Kwak, and Young-Ho Jung. Multi-mode SDR radar platform for small air-vehicle drone detection. In *2016 CIE International Conference on Radar (RADAR)*. IEEE, oct 2016. doi: 10.1109/radar.2016.8059254.

[11] Nadav Levanon and Eli Mozeson. *Radar Signals*. John Wiley & Sons, Inc., jul 2004. doi: 10.1002/0471663085.

[12] Themba W Mathumo, Theo G Swart, and Richard W Focke. Implementation of a gnu radio and python fmcw radar toolkit. In *2017 IEEE AFRICON*, pages 585–590. IEEE, 2017.

[13] Erik George Moore. Radar detection, tracking and identification for uav sense and avoid applications. Master's thesis, University of Denver, 2019. Electronic Theses and Dissertations. 1544. https://digitalcommons.du.edu/etd/1544/.

[14] Mark A. Richards, James A. Scheer, and William A. Holm. *Priniciple of Modern Radar*, volume 1. SciTech Publishing, 2010.

[15] Sundaresan S, Anjana C, Tessy Zacharia, and Gandhiraj R. Real time implementation of FMCW radar for target detection using GNU radio and USRP. In *2015 International Conference on Communications and Signal Processing (ICCSP)*. IEEE, apr 2015. doi: 10.1109/iccsp.2015.7322772.

[16] Merrill I. Skolnik. *Radar Handbook*. McGraw-Hill Education Ltd, 2008.

[17] Wally H. W Tuttlebee. *Software defined radio: enabling technologies*. Wiley, 2002.

[18] Fawwaz T. Ulaby and Umberto Ravaioli. *Fundamentals of Applied Electromagnetics*. Always learning. Pearson, Boston [u.a.], 7th ed., global ed. edition, 2015.

[19] Nicholas J Willis. *Bistatic Radar*, volume 2. SciTech Publishing, 2005.

[20] Qizhao Zhu and Yaqi Wang. Fmcw radar implemented with gnu radio companion, 2016.